Modeling and Numerical Analysis for Catalytic Membrane Reactors

by

Nagima Chalkarova

Submitted to the Department of Mathematics
in partial fulfillment of the requirements for the degree of

Master of Science in Applied Mathematics

at the

NAZARBAYEV UNIVERSITY

May 2020

Author .....
Department of Mathematics
May 6, 2020

Certified by .....
Piotr Skrzypacz
Assistant Professor
Thesis Supervisor

Accepted by .....
Daniel Pugh
Dean, School of Sciences and Humanities

Modeling and Numerical Analysis for Catalytic Membrane Reactors

by

Nagima Chalkarova

Submitted to the Department of Mathematics
on May 6, 2020, in partial fulfillment of the
requirements for the degree of
Master of Science in Applied Mathematics

Abstract

There has been great interest in membrane reactors over the last decades. The limitation of selectivity and yield of certain products in chemical reactions is an important and not sfficiently solved problem in the field of Chemical Reaction Engineering. One possible way to circumvent this problem is through the use of membrane reactors. Compared to conventional reactors, catalytic membrane reactors have significantly improved performance. In this study the mathematical model employed is based on the coupled convection-diffusion-reaction equations with temperature-dependent reaction coefficients. By using the modified Crank-Nicolson scheme the problem is solved numerically. The numerical approximation is compared to one obtained by the collocation-based *pdepe* Matlab solver. This renowned Matlab solver fails to compute solutions in the case of large system parameters whereas the modified Crank-Nicolson method copes with the case of large Thiele modulus parameter. The proposed method has unconditional stability and second order of accuracy with respect to both space and time. Since the non-isothermal model has nonlinear power-law kinetics of fractional order, the existence of dead zones is also investigated. The effects of parameters such as reaction order, Peclet number, Thiele modulus on solution profiles are studied. The results show that these parameters influence the appearance of the dead zone in the non-isothermal multi-component reaction. Our parameter studies indicate that there exists a critical value of the Thiele modulus for each component in a consecutive irreversible reaction. Also, the effects of dimensionless Peclet number and Thiele modulus on selectivity, yield of intermediate product and conversion are analyzed. The effect of Peclet number is more significant for small values of Thiele modulus. We also find that, increasing convective flow, the conversion decreases and the increasing Thiele modulus leads to the increase of conversion.

Thesis Supervisor: Piotr Skrzypacz
Title: Assistant Professor

Acknowledgments

I wish first like to express my sincere appreciation to my supervisor, Professor Piotr Sebastian Skrzypacz of the School of Sciences and Humanities at Nazarbayev University. He has provided me with all necessary reading materials and extensive support from the beginning of working on my thesis till the end. Prof. Skrzypacz guided me in the right directions and gave valuable and constructive suggestions during the planning and development of the thesis.

I would also like to thanks Professor Boris Golman of the School of Engineering and Digital Sciences at Nazarbayev University as the co-advisor, for providing me with with his papers and for his advice during regular meetings.

Finally, I wish to acknowledge the great love and support of my family. They kept me going on and supported throughout my study.

Contents

Nomenclature

Alphabet

B^e	effective permeabiltiy	m^2
C_i	concentration for component i in membrane	mol/m^3
$C_{i,0}$	concentration for i component in feed stream	mol/m^3
$C_{i,L}$	concentration for i component in exhaust stream	mol/m^3
C_i^*	concentration of i in dimensionless form	$-$
c_p	specific heat of fluid	$J/(mol \cdot K)$
D_i^e	effective diffusivity for component i	m^2/s
E_i	activation energy	J/mol
$-\Delta H_\rho$	heat of reaction ρ per mole for component A	J/mol
K^e	effective thermal conductivity	$J/(mol \cdot s \cdot K)$
k_ρ	for reaction ρ reaction rate constant	$1/s$
k_ρ^0	for reaction ρ reaction rate constant evaluated at gas phase temperature T_0	$1/s$
L	thickness of membrane	m
N_i	total molar flux for i species per unit cross-sectional area of membrane	$mol/(m^2 \cdot s)$
N_i^D	diffusive molar flux for i species per unit cross-sectional area of membrane	$mol/(m^2 \cdot s)$
P	pressure inside membrane	Pa
Pe_m	mass Peclet number	$-$
Pe_h	heat Peclet number	$-$
q	heat flux per unit cross-sectional area of membrane	$J/(m \cdot s)$
R_G	universal gas constant	$J(mol \cdot K)$
R_i	molar reaction rate for component i per unit volume of porous membrane	$mol/(m^3 \cdot s)$
r_ρ	volumetric reaction rate for reaction ρ	$mol/(m^3 \cdot s)$
S	selectivity for component B	$-$
T	temperature inside membrane	K
T_0	gas phase temperature at feed stream	K
t	time	s
u_D	filter velocity with porous material	m/s
X	conversion for component A	
x	distance variable	m
Y	yield for component B	$-$
z	dimensionless distance	$-$

Greek Symbols

β_1, β_2	Prater numbers	$-$
γ_1, γ_2	Arrhenius numbers	$-$
θ	dimensionless temperature	$-$
μ	dynamic viscosity of fluid phase	$kg/(m \cdot s)$
ξ	ratio of reaction rate	$-$
ρ_g	density of fluid	kg/m^3
$\varsigma_{i\rho}$	stoichiometric coefficient for species i in reaction ρ	$-$
ϕ	Thiele modulus	$-$
ψ	diffusivity ratio	$-$

Chapter 1

Introduction

A membrane reactor (MR) is a device that combines a membrane separation or distribution process with a chemical reaction in single unit [1]. This term was started to use in chemical processing literature approximately in 1980 [1]. Over the last decades, the interest in the membrane reactors increased. The limitation of the selectivity and yield of the certain products in reactions is an important and not sufficiently solved problem in the field of Chemical Reaction Engineering. Use of membrane reactors can be considered as one of possible ways to solve this problem. Compared with conventional reactors, the membrane reactors can significantly improve performance of chemical reactions. This is due to the membrane inside the reactor which divides it into two sides: shell and tube [2].

1.1 Membrane Types for Membrane Reactors

There are different types of membranes. They are categorized according to their nature, separation regime and shape. By nature they are divided into synthetic and biological. They differ for functionality and the structure of membrane itself. Biological membranes have drawbacks like limited pH range and operating temperature, sensitivity to microbes. But their advantage is that they are easily produced. Synthetic membranes can be divided into organic and inorganic. Usually inorganic membrane can be used above 250°C, while organic membranes operate from 100-300°C [3]. Also,

inorganic membranes are classified as porous and dense membranes. While porous membrane has high permeability and low selectivity, dense membranes have opposite. Porous membranes are distinguished depending on the pore size [2].

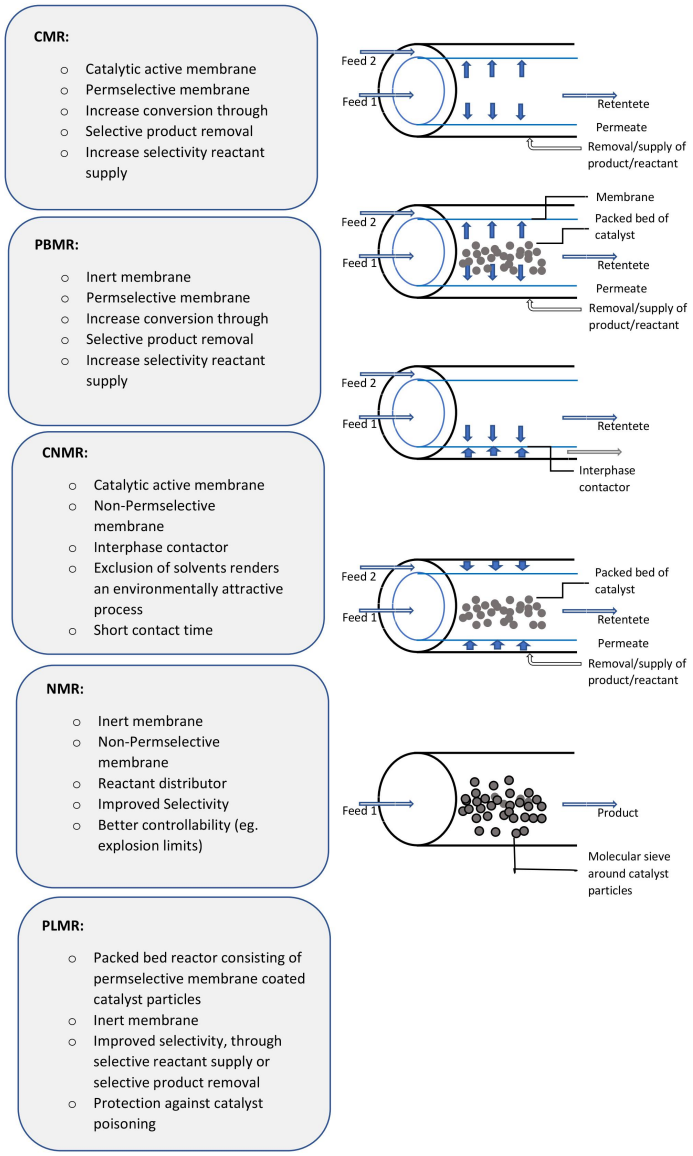

Figure 1-1: Categorization of MRs based on the functionality and location of membrane.Adapted from "Membranes for membrane reactors: preparation, optimization and selection.", by A. Basile and F. Gallucci (Eds.), 2010,John Wiley & Sons. [3]

Basile and Gallucci in their work divided MRs into the classes based on the location and function of membrane , as seen in Figure 1-1:

- Catalytic membrane reactor (CMR)
- Catalytic non-permselective membrane reactor (CNMR)
- Packed-bed membrane reactor (PBMR)
- Packed-bed catalytic membrane reactor (PBCMR)
- Fluidized-bed membrane reactor (FBMR)
- Fluidized-bed catalytic membrane reactor (FBCMR)
- Nonperm-selective membrane reactors (NMR)
- Reactant-selective packed bed reactors (RSPBR) [3].

1.2 Catalytic Membrane Reactors

In this work, a catalytic membrane reactor (CMR) is considered. CMR is a device where membrane works as separation layer and as catalyst at the same time. In CMR there are four ways to locate catalysts in the membrane. Figure 1-2 represents these four ways [4].

In Figure 1-2, (a), the catalyst is physically divided from an inert membrane [4]. In this case, we can separately modulate functions for the catalyst activity and the membrane. The catalyst pellets are usually packed on the inert membrane and it is the most popular in practice [4]. In addition, catalysts can be placed not on the separation layer, but they can be located on another side of membrane. Usually it is due to the harm of catalysts on separation layer.

In (b), the surface of membrane is covered with catalyst. The catalyst past is used here and it is integrated with the membrane into a single body.

In (c), it is shown that catalyst is dispersed in the porous substrate of the membrane [4]. In comparison with classical reactors, the conversion of reactants, the access

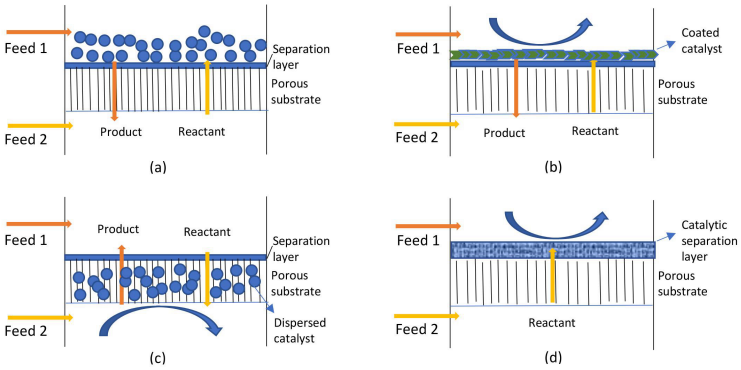

Figure 1-2: Location of catalysts in CMR: (a) the catalyst is physically divided from an inert membrane; (b) catalyst is coated on the surface of membrane; (c) catalyst is dispersed in porous substrate of the membrane; (d) inherently catalytic membrane. Adapted from "Inorganic Membrane Reactors, Second edition.", by X. Tan, 2015,Wiley:China, UK, pp 1- 25, 143-179. [4]

of reactants to catalysts and catalytic efficiency are higher in this type of catalytic porous membrane reactors. It is illustrated in Figure 1-3.

Figure 1-2, (d) shows inherently catalytic membrane type. The membrane is made of catalytic material and the membrane operates both as catalyst and as separator membrane as well. It controls both important functions of the reactor simultaneously [4].

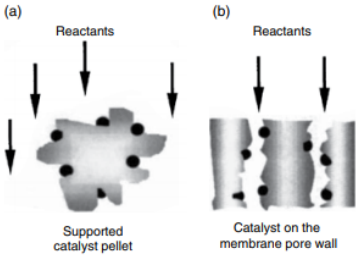

Figure 1-3: Reactants flow in (a) a catalytic pellet and (b) a catalytic porous membrane, catalysts are located in the walls of pores. Adapted from "Inorganic Membrane Reactors, Second edition.", by X. Tan, 2015,Wiley:China, UK, pp 1- 25, 143-179. [4]

1.3 Dead Zones

The dead core is defined as a zone where full consumption of reactants occurs and no reaction is held [15]. It is very important to know where the dead zone appears. It allows us to use the expensive catalyst material efficiently and reduce reactor costs [16].

There are many works and vast literature about dead zones. One of them is the work of Andreev [5]. He investigated the formation of dead zones for porous structures with the processes under non-steady and steady-state conditions. According to his definition of a dead zone, it is a place in porous material where reactants can not penetrate. The necessary conditions for the appearance of the dead core were derived analytically. He also showed that there is a critical value of the Thiele modulus which determines the existence of the dead zone. If the Thiele modulus is bigger or equal to its critical value, then the dead zone can be formed. In [12] the necessary conditions were established for consecutive, parallel, and almost for all chemical reactions in cylindrical, spherical porous catalyst pellets.

Solutions with dead-core and without for diffusion-reaction problems were studied by Skrzypacz et al [11]. The main goal was to derive a semi-analytic solution for the diffusion-reaction problem with power-law kinetics. Also, they considered different pellet geometries. In the case of the power-law nonlinear term, the concentration profile was investigated. All the effects of some parameters such as, Thiele modulus, the geometry of the pellets, reaction order, and Biot number, which can influence concentration were showed through the graphs. For example by increasing reaction order, Thiele modulus concentration profile decreases. In their study the largest dead zone was formed for planar geometry.

One more paper which can be considered is based on the formation of dead zones in a porous catalyst with temperature-dependent diffusion under nonisothermal condition. Andreev et al. [12] have derived analytically critical Thiele modulus as sufficient conditions for the formation of the dead zone. The parameters which influence Thiele modulus are described and examined numerically. Due to the coefficient of

temperature-dependent diffusion, the critical Thiele modulus differs from the equations derived by Andreev [5], Sabit et al. [10]. It was concluded that an increase of Arrhenius number for diffusion and a decrease of Arrhenius number for reaction leads to the increase of critical Thiele modulus. Additionally, critical Thiele modulus has the highest value in pellets with spherical geometry and the lowest for planar geometry. Despite the fact that the formation of the dead zones was investigated in many works, the appearance of dead-zones in convection-diffusion-reaction problems is still an unexplored area of research.

This study is aimed to solve numerically convection-diffusion-reaction problem under nonisothermal conditions and investigate process parameters which have effects on the solution profiles and the appearance of the dead zone since the power-law kinetics are used. Also, the performance of a one-dimensional model for catalytic membrane reactors will be evaluated.

Chapter 2

Mathematical Model

Mathematical modeling is useful for design and construction of commercial chemical reactors. Models can predict behavior of the system and find the optimal process conditions. This can significantly reduce reactor costs. Mathematical modeling of processes in catalytic membrane reactors is also one of the ways to reduce the number of experiments. It gives a chance to evaluate a significant number of parameters on which process indicators, such as conversion, selectivity, and yield, depend. These parameters are usually the temperature, concentration of reactants, time, and reaction rates. The results of reactor modeling and analysis allow developing some recommendations regarding structural design of reactors and to define optimal conditions for processes.

2.1 General Case

In this study a one-dimensional catalytic membrane reactor model is introduced. The porous membrane with catalysts impregnated inside of the pore walls is used. Figure 2-1 shows a scheme of chosen membrane reactor which is adapted from the paper of Golman et al. [6]. In Figure 2-1, a tube has one closed end at the bottom. The membrane is U-shaped and the reactants go directly from the inner side of membrane. They are fed to the reaction in the porous membrane, and then products and unconverted reactants are removed from the outside of the membrane.

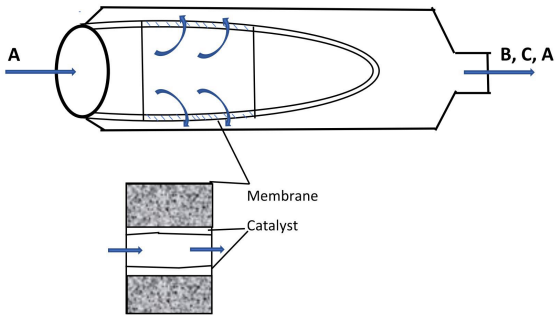

Figure 2-1: Schematic representation of porous CMR. Adapted from "Selectivity and yield of exothermic consecutive reactions in catalytically active porous membrane reactor",by B. Golman et al.,1997,Journal of chemical engineering of Japan, 30(3), 507-513. [6].

For better understanding of the reaction, the mathematical model of the catalytic membrane reactor is considered.In this study, it is based on the model form paper of Golman, Shinohara, and Kobayashi [6]. There are assumptions regarding the model, like high permeability of membrane, small membrane thickness, and reactant's rate of flow is high. The homogeneous model is presented in plane geometry with transfer of mass and heat in catalytically active and porous membrane.

The consecutive irreversible reaction under nonisothermal condition is considered in the present study

$$A \xrightarrow{k_1} B \xrightarrow{k_2} C \tag{2.1}$$

A is the reactant, which is fed to the membrane pore from the inner side of catalytic membrane, B is the desired product, which escapes from outer side of membrane before further converting to C.

The steady-state mass balance for the i-th gaseous species and heat balance are expressed by the following equations

$$\frac{dN_i}{dx} - R_i = 0 \tag{2.2}$$

and

$$\frac{dq_i}{dx} - \sum_{\rho}(- \triangle H)_{\rho} r_{\rho} = 0\,, \tag{2.3}$$

where, N_i is the molar flux of component i per unit total cross sectional area; x is position or distance; R_i is the molar reaction rate of i-th species per unit volume; q is the heat flux ; $(- \triangle H)_{\rho}$ is the heat of ρ-th reaction per mole of the $i-th$ component. The molar reaction rate R_i is given by

$$R_i = \sum_{\rho} \zeta_{i\rho} r_{\rho}\,.$$

The total molar flux of a gas through porous membrane is given by the sum of an effective diffusion term and convective transport term assuming they are independent from each other. This results in

$$N_i = N_i^D + u_D C_i\,. \tag{2.4}$$

In this study, Fick's flux model is used. The components are moved to a porous medium by total pressure and mole fraction gradients. In order to simplify the problem the diffusion flux is described by Fick's law and is expressed by the following equation

$$N_i^D = -D_i^e \frac{dC_i}{dx}, \tag{2.5}$$

where, D_i^e is the effective diffusion coefficient of i-th component inside the membrane. In this model the temperature and pressure do not affect diffusivity. Because the pressure variation is not high and reaction rates are given by Arrhenius equation.
The Darcian fluid velocity u_D is given as

$$u_D = -\frac{B^e}{\mu}\frac{dP}{dx}, \tag{2.6}$$

where, B^e is the effective permeability of the pore; $\frac{dP}{dx}$ is the pressure gradient. Along the flow, the uniform field of velocity inside may be assumed with the constant of mean pressure gradient. Because the pressure variation, which cause bulk flow, is

smaller than the total pressure and the temperature variation does not affect filter velocity.

Inserting Eq. (2.5) into Eq. (2.4), yields the total molar flux

$$N_i = -D_i^e \frac{dC_i}{dx} + u_D C_i \,. \tag{2.7}$$

The total heat flux is expressed as

$$q = -K^e \frac{dT}{dx} + \rho_g c_p u_D T, \tag{2.8}$$

where, K^e is the effective thermal conductivity.

Then by replacing Equations (2.7) and (2.8) in mass and energy balance equations (2.2) and (2.3), we get

$$D_i^e \frac{d^2 C_i}{dx^2} - u_D \frac{dC_i}{dx} + R_i = 0 \,, \tag{2.9}$$

and

$$K_i^e \frac{d^2 T_i}{dx^2} - \rho_g c_p u_D \frac{dT_i}{dx} + \sum_\rho (- \triangle H)_\rho r_\rho = 0 \,. \tag{2.10}$$

In the reaction model (2.1), the chemical reaction kinetics has to be included. In our case of the he first order irreversible consecutive reactions, the reaction terms are described by

$$R_A = -r_1 \quad \text{and} \quad R_B = -r_2 + r_1 \,,$$

where r_i denotes the reaction rate. In general, the reaction rates depend on temperature and the molar concentrations $r = r(T, c_1, c_2, c_3, ...)$. We use the Arrhenius equation to specify the rate constant as follows

$$k_i = k_i^0 e^{-\frac{E_i}{R_G}(\frac{1}{T} - \frac{1}{T_0})} \,.$$

Here, k_i^0 stands for the preexponential constant, E_i is activation energy and R_G denotes universal gas constant, see [2]. In this work, the reaction rates are prescribed as $r_1 = k_1 C_A^p$ and $r_2 = k_2 C_B^p$, where the fractional reaction exponent $p \in (0, 1)$ is

obtained experimentally. Then, the system of nonlinear differential equations becomes

$$D_A^e \frac{d^2 C_A}{dx^2} - u_D \frac{dC_A}{dx} - k_1^0 e^{-\frac{E_i}{R_G}(\frac{1}{T}-\frac{1}{T_0})} C_A^p = 0\,, \tag{2.11}$$

$$D_B^e \frac{d^2 C_B}{dx^2} - u_D \frac{dC_B}{dx} - k_2^0 e^{-\frac{E_i}{R_G}(\frac{1}{T}-\frac{1}{T_0})} C_B^p + k_1^0 e^{-\frac{E_i}{R_G}(\frac{1}{T}-\frac{1}{T_0})} C_A^p = 0\,, \tag{2.12}$$

$$K^e \frac{d^2 T}{dx^2} - \rho_g c_p u_D \frac{dT}{dx} + k_1^0 e^{-\frac{E_i}{R_G}(\frac{1}{T}-\frac{1}{T_0})} C_A^p (- \triangle H_1) + k_2^0 e^{-\frac{E_i}{R_G}(\frac{1}{T}-\frac{1}{T_0})} C_B^p (- \triangle H_2) = 0\,. \tag{2.13}$$

The Dirichlet boundary conditions are imposed at $x = 0$

$$C_A = C_{A,0}, \quad C_B = 0, \quad T = T_0\,,$$

where $C_{A,0}$ and T_0 are the prescribed concentration and temperature at the boundary, respectively. At $x = L$ the following boundary conditions are imposed

$$\frac{dC_A}{dx} = \frac{dC_B}{dx} = 0, \quad \frac{dT}{dx} = 0\,.$$

2.2 Dimensionless Model Equations

In order to rewrite Equations (2.11), (2.12) and (2.13) in dimensionless form, the dimensionless paramters defined in Table 2.1 are used. The following equations describe the steady-state mass balance after nondimensionalization

$$\frac{d^2 C_A^*}{dz^2} - Pe_m \frac{dC_A^*}{dz} - \phi^2 \frac{\xi}{\psi} e^{\gamma_1(1-\frac{1}{\theta})} C_A^{*p} = 0\,, \tag{2.14}$$

$$\frac{d^2 C_B^*}{dz^2} - Pe_m \psi \frac{dC_B^*}{dz} - \phi^2 e^{\gamma_1(1-\frac{1}{\theta})} C_B^{*p} + \phi^2 \xi e^{\gamma_2(1-\frac{1}{\theta})} C_A^{*p} = 0\,. \tag{2.15}$$

The energy balance is described by the following dimensionless equation

Table 2.1: Dimensionless parameters [6]

Parameter	**Definition**
Peclet number for mass	$Pe_m = \frac{L \cdot u_D}{D_A^e}$
Peclet number for heat	$Pe_h = \frac{\rho_g \cdot c_p \cdot u_D \cdot L}{K^e}$
Thiele modulus	$\phi = \sqrt{\frac{L^2 \cdot k_2^0 \cdot C_{A,0}^{p-1}}{D_B^e}}$
Ratio for reaction rate	$\xi = \frac{k_1^0}{k_2^0}$
Ratio for effective diffusivity	$\psi = \frac{D_A^e}{D_B^e}$
Energy generation function	$\beta_1 = \frac{(-\Delta H_1) \cdot D_A^e \cdot C_{A,0}}{K^e \cdot T_0}$
	$\beta_2 = \frac{(-\Delta H_2) \cdot D_B^e \cdot C_{A,0}}{K^e \cdot T_0}$
Arrhenius numbers	$\gamma_1 = \frac{E_1}{R_G \cdot T_0}$
	$\gamma_2 = \frac{E_2}{R_G \cdot T_0}$

$$\frac{d^2\theta}{dz^2} - Pe_h \frac{d\theta}{dz} + \beta_1 \phi^2 \frac{\xi}{\psi} e^{\gamma_1(1-\frac{1}{\theta})} C_A^{*p} + \beta_2 \phi^2 e^{\gamma_2(1-\frac{1}{\theta})} C_B^{*p} = 0\,. \tag{2.16}$$

The mass and energy balance equation (2.14)-(2.16) are complemented by the boundary conditions

$$\text{at} \quad z = 1: \qquad C_A^* = 1, \quad C_B^* = 0, \quad \theta = 1\,, \tag{2.17}$$

and

$$\text{at} \quad z = 0: \qquad \frac{d\theta}{dz} = \frac{dC_A^*}{dz} = \frac{dC_B^*}{dz} = 0\,. \tag{2.18}$$

Here, $C_A^* = \frac{C_A}{C_{A,0}}$; $\quad C_B^* = \frac{C_B}{C_{A,0}}$ are the pdimensionless concentrations for components A and B, $z = \frac{x}{L}$ is the dimensionless spatial coordinates, and $\theta = \frac{T}{T_0}$ stands for the dimensionless temperature.

Chapter 3

Numerical Approach

3.1 Analytic Solution for Linear Steady-state Equation

Let us consider the following steady-state one-component equation

$$\frac{d^2c}{dz^2} - Pe_m\frac{dc}{dz} - bc = 0, \tag{3.1}$$

where c is the dimensionless concentration, z is the dimensionless distance, $b > 0$ is reaction rate constant and Pe_m is the dimensionless Peclet number defined as

$$Pe = \frac{u_D L}{D_A}\,.$$

The boundary conditions are

at z=0:

$$c = 1 \tag{3.2}$$

at z=1:

$$\frac{dc}{dz} = 0 \tag{3.3}$$

Equation (3.1) is the second order linear differential equation. In the following, we will derive its analytic solution. The characteristic equation for Eq. (3.1) reads as

follows

$$k^2 - Pe_m k - b = 0\,,$$

and it has two real roots

$$k_{1/2} = \frac{Pe_m \pm \sqrt{Pe_m^2 + 4b}}{2}\,. \tag{3.4}$$

Then, the general solution is given by

$$c(z) = C_1 e^{k1*z} + C_2 e^{k2*z}\,, \tag{3.5}$$

where the constants $C_1, C_2 \in \mathbb{R}$ will be determined from the boundary conditions stated by Eq.(3.2)and Eq.(3.3). We have $c(0) = 1 \Rightarrow c(0) = C_1 e^{0\cdot k1} + C_2 e^{0\cdot k2}$, so

$$C_1 = 1 - C_2\,, \tag{3.6}$$

and $\frac{dc}{dz}(1) = 0 \Rightarrow \frac{dc}{dz}(z) = C_1 k_1 e^{k1*z} + C_2 k_2 e^{k2*z}$, so

$$C_1 k_1 e^{k1} = -C_2 k_2 e^{k2}\,. \tag{3.7}$$

Using Eq. (3.6), it follows from Eq. (3.7) that

$$C_2 = \frac{1}{1 - \frac{k_2}{k_1} e^{k2-k1}} \tag{3.8}$$

and

$$C_1 = 1 - \frac{1}{1 - \frac{k_2}{k_1} e^{k2-k1}}\,. \tag{3.9}$$

The Equations (3.4), (3.8) and (3.9) are inserted into Eq.(3.5). Then, the analytic solution to the one-component linear model equation (3.1) is given by

$$c(z) = \left[-\frac{(Pe_m + \sqrt{Pe_m^2 + 4b}) \cdot e^{\sqrt{Pe_m^2+4b}}}{Pe_m - \sqrt{Pe_m^2 + 4b} - (Pe_m + \sqrt{Pe_m^2 + 4b}) \cdot e^{\sqrt{Pe_m^2+4b}}} \right] \cdot e^{\frac{Pe_m - \sqrt{Pe_m^2+4b}}{2} z} + \left[\frac{Pe_m - \sqrt{Pe_m^2 + 4b}}{Pe_m - \sqrt{Pe_m^2 + 4b} - (Pe_m + \sqrt{Pe_m^2 + 4b}) e^{\sqrt{Pe_m^2+4b}}} \right] \cdot e^{\frac{Pe_m + \sqrt{Pe_m^2+4b}}{2} z} . \tag{3.10}$$

3.2 Finite Difference Scheme for Linear Steady-state Equation

In the following, we will establish the finite difference scheme for the boundary value problem Eq.(3.1)-(3.3) using the spatial grid, $z_0 = 0 < z_1 < z_2 < ... < z_N < z_{N+1} = L$. For simplicity, we place the grid points uniformly with $h = \Delta z = \frac{1}{N+1}$.

3.2.1 Central Difference Scheme (CDS)

The second derivative at the grid point $z = z_i$ is approximated by the second central difference quotient

$$\frac{d^2c}{dz^2}(z_i) = \frac{c_{i-1} - 2c_i + c_{i+1}}{h^2} + \mathcal{O}(h^2)\,, \tag{3.11}$$

where $\mathcal{O}(h^2)$ is the order of the truncation error.
The first derivative of $c(z)$ at the grid point z_i is approximated using central difference quotient

$$\frac{dc}{dz}(z_i) = \frac{c_{i+1} - c_{i-1}}{2h} + \mathcal{O}(h^2)\,. \tag{3.12}$$

Then, we can write CDS equation for the i-th grid point as

$$\frac{c_{i-1} - 2c_i + c_{i+1}}{h^2} - \frac{Pe_m}{2h}\big(c_{i+1} - c_{i-1}\big) - bc_i = 0\,,$$

and consequently obtain

$$\left(\frac{1}{h^2}+\frac{Pe_m}{2h}\right)c_{i-1}+\left(-\frac{2}{h^2}-b\right)c_i+\left(\frac{1}{h^2}-\frac{Pe_m}{2h}\right)c_{i+1}=0\,. \tag{3.13}$$

Define α, β and γ as

$$\alpha=\frac{1}{h^2}+\frac{Pe_m}{2h};\quad \beta=\frac{1}{h^2}-\frac{Pe_m}{2h};\quad \gamma=-\frac{2}{h^2}-b\,.$$

Now, we take into account the boundary conditions. At the boundary point $z=0$, we have $c_0=1$. Thus, we have for $i=1$:

$$\gamma c_1+\beta c_2=-\alpha\,.$$

At the boundary point $z=1$ the Neumann boundary condition is imposed. Using the central difference quotient Eq.(3.12), we have

$$\frac{dc}{dz}|_{z=1}\approx\frac{c_{N+1}-c_{N-1}}{2h}=0\,. \tag{3.14}$$

From the above Eq.(3.14), we get formula for c_{N+1}:

$$c_{N+1}-c_{N-1}=0\,,$$

and so

$$c_{N+1}=c_{N-1}\,. \tag{3.15}$$

Now, we consider difference equation Eq.(3.13) for $i=N$:

$$\alpha c_{N-1}+\gamma c_N+\beta c_{N+1}=0\,. \tag{3.16}$$

In Eq.(3.16) c_{N+1} is replaced by c_{N-1} due to Eq.(3.15). Then, Eq.(3.16) becomes as follows

$$(\alpha+\beta)c_{N-1}+\gamma c_N=0\,,$$

and we obtain

$i = 1$:

$$\gamma c_1 + \beta c_2 = -\alpha\,,$$

$i = 2$:

$$\alpha c_1 + \gamma c_2 + \beta c_3 = 0\,,$$

$i = 3$:

$$\alpha c_2 + \gamma c_3 + \beta c_4 = 0\,,$$

$\vdots$

$i = N$:

$$(\alpha + \beta) c_{N-1} + \gamma c_N = 0\,.$$

Consequently,

$$\begin{pmatrix} \gamma & \beta & & 0 & \\ \alpha & \ddots & \ddots & & \\ & \ddots & \ddots & \ddots & \\ & & \alpha & \gamma & \beta \\ 0 & & & \alpha+\beta & \gamma \end{pmatrix} \begin{pmatrix} c_1 \\ c_2 \\ \vdots \\ c_N \end{pmatrix} = \begin{pmatrix} -\alpha \\ 0 \\ \vdots \\ 0 \end{pmatrix}.$$

Fig. 3-1 shows numerical and analytic solution of our steady-state mass balance equation, Eq. (3.1). It is well known fact that the numerical solution obtained from CDS can have large oscillations for the high Peclet numbers. However, CDS produces a stable numerical solution to our problem, see Fig. 3-1. This can be justified by the fact that the exact solution to our problem exhibits no boundary layers.

3.2.2 Backward Difference Scheme (BDS)

For the second derivative, we use the following approximation from Eq. (3.11). The first derivative of $c(z)$ at the grid point z_i is approximated as follows

$$\frac{dc}{dz} = \frac{c_i - c_{i-1}}{h} + \mathcal{O}(h)\,. \tag{3.17}$$

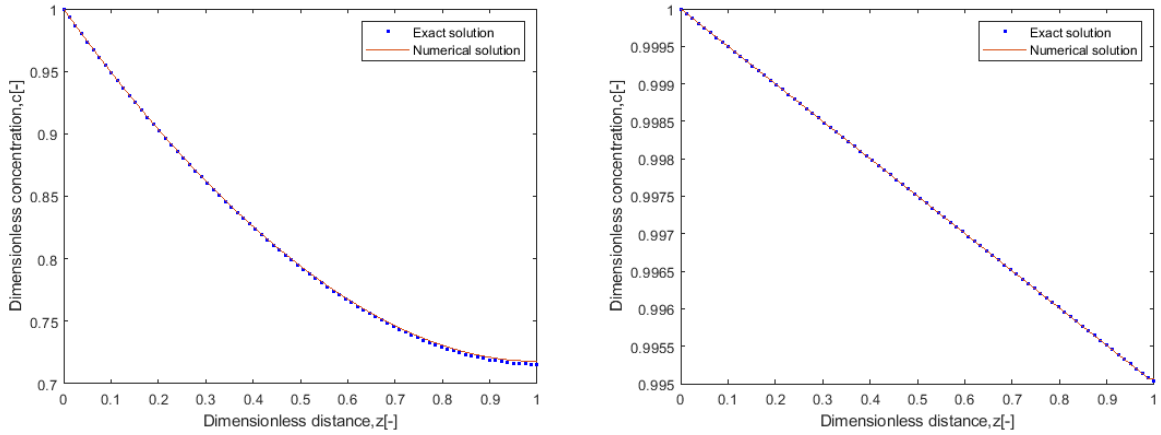

(a) (b)

Figure 3-1: Dimensionless concentration calculated by analytical and central difference method: (a) $Pe_m = 1, b = 1$, (b) $Pe_m = 200, b = 1$.

Then, the BDS equation for the i-th grid point is given by

$$\left(-\frac{2}{h^2} - \frac{Pe_m}{h} - b\right) c_i + \left(\frac{1}{h^2} + \frac{Pe_m}{h}\right) c_{i-1} + \frac{1}{h^2} c_{i+1} = 0\,. \tag{3.18}$$

Let us apply the backward difference quotient in order to approximate BC's stated by Eq.(3.3). By combining Eq.(3.17) with the boundary condition at $z = 1$, we get

$$\frac{c_i - c_{i-1}}{h} = 0\,. \tag{3.19}$$

From the above Eq.(3.19), we get the relation for c_{N+1}, namely

$$c_{N+1} - c_N = 0\,,$$

and consequently

$$c_{N+1} = c_N\,. \tag{3.20}$$

Define α, β and γ as follows

$$\alpha = -\frac{2}{h^2} - \frac{Pe_m}{2} - b; \quad \beta = \frac{1}{h^2}; \quad \gamma = \frac{1}{h^2} + \frac{Pe_m}{h}$$

Also, from the boundary conditions we infer that $c_0 = 1$:

$i = 1$:

$$\alpha c_1 + \gamma + \beta c_2 = 0\,.$$

In the equation for $i = N$, we express c_{N+1} as in Eq.(3.20):

$$\left(-\frac{2}{h^2} - \frac{Pe_m}{2} - b\right) c_N + \left(\frac{1}{h^2} + \frac{Pe_m}{h}\right) c_{N-1} + \frac{1}{h^2} c_N = 0\,,$$

$$\left(-\frac{1}{h^2} - \frac{Pe_m}{2} - b\right) c_N + \left(\frac{1}{h^2} + \frac{Pe_m}{h}\right) c_{N-1} = 0\,,$$

$$d = -\frac{1}{h^2} - \frac{Pe_m}{2} - b; \quad l = \frac{1}{h^2} + \frac{Pe_m}{h}\,.$$

Then, the following tridiagonal matrix is obtained

$$\begin{pmatrix} \alpha & \beta & & & 0 \\ \gamma & \ddots & \ddots & & \\ & \ddots & \ddots & \ddots & \\ & & \gamma & \alpha & \beta \\ 0 & & & l & d \end{pmatrix} \begin{pmatrix} c_1 \\ c_2 \\ \vdots \\ c_N \end{pmatrix} = \begin{pmatrix} -\gamma \\ 0 \\ \vdots \\ 0 \end{pmatrix}$$

Despite the fact that BDS approximates convection derivative less accurate than central difference method, it behaves better and more stable in the case of the hight Peclet numbers. However, in this study both variants of finite difference method perform well, see Fig. 3-1 and 3-2.

3.2.3 Exact Finite Difference Solution

In the following, we will derive the formula for the exact solution to the BDS. Notice that the BDS equation (3.18) for the grid point i is

$$\left(-\frac{2}{h^2} - \frac{Pe_m}{h} - b\right) c_i + \left(\frac{1}{h^2} + \frac{Pe_m}{h}\right) c_{i-1} + \frac{1}{h^2} c_{i+1} = 0\,.$$

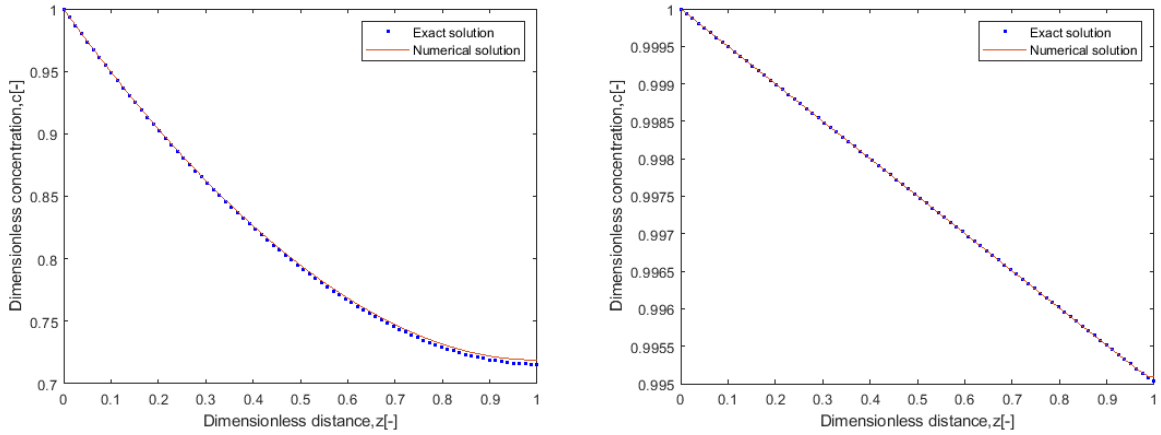

(a) (b)

Figure 3-2: Dimensionless concentration calculated by analytical and backward difference method: (a) $Pe_m = 1, b = 1$, (b) $Pe_m = 200, b = 1$.

The boundary conditions are

at z=0:

$$c = 1\,,$$

at z=1:

$$\frac{dc}{dz} = 0\,.$$

In order to solve the above linear difference equation, let us assume that $u_i = \lambda^i$ and put it into the Eq. (3.18). We have

$$\left(-\frac{2}{h^2} - \frac{Pe_m}{h} - b\right)\lambda^i + \left(\frac{1}{h^2} + \frac{Pe_m}{h}\right)\frac{\lambda^i}{\lambda} + \frac{1}{h^2}\lambda^i \cdot \lambda = 0\,.$$

Multiplying this equation by $\frac{\lambda \cdot h^2}{\lambda^i}$ yields

$$\lambda^2 + (-2 - Pe_m h - bh^2)\lambda + (1 + Pe_m h) = 0\,.$$

The roots of the above quadratic equation are

$$\lambda_{1/2} = \frac{Pe_m h + 2 + bh^2 \pm \sqrt{(-Pe_m h - 2 - bh^2)^2 - 4 - 4Pe_m h}}{2}\,.$$

Both of the roots are positive and general solution of the difference equation is given by

$$c_i = A\lambda_1^i + B\lambda_2^i \,.$$

Applying the boundary conditions yields

at z=0:

$$c_0 = A\lambda_1^0 + B\lambda_2^0 = 1 \,,$$

$$B = 1 - A \,, \tag{3.21}$$

at z=1:

$$\frac{dc}{dz}(z_n) = \frac{c_n - c_{n-1}}{h} = 0 \,, \tag{3.22}$$

so

$$c_n = c_{n-1} \,.$$

We express c_n and c_{n-1} by general solution Eq.(3.21) and coefficient B by Eq.(3.22)

$$A\lambda_1^n + (1-A)\lambda_2^n = A\lambda_1^{n-1} + (1-A)\lambda_2^{n-1} \,.$$

From this equation, it follows that the coefficients A and B are given by

$$A = \frac{\lambda_2^{n-1} - \lambda_2^n}{\lambda_1^n - \lambda_2^n - \lambda_1^{n-1} + \lambda_2^{n-1}} \,,$$

$$B = \frac{\lambda_1^n - \lambda_1^{n-1}}{\lambda_1^n - \lambda_2^n - \lambda_1^{n-1} + \lambda_2^{n-1}} \,.$$

Then, the general solution for the difference equation is

$$c_i = \frac{\lambda_2^{n-1} - \lambda_2^n}{\lambda_1^n - \lambda_2^n - \lambda_1^{n-1} + \lambda_2^{n-1}} \cdot \lambda_1^i + \frac{\lambda_1^n - \lambda_1^{n-1}}{\lambda_1^n - \lambda_2^n - \lambda_1^{n-1} + \lambda_2^{n-1}} \cdot \lambda_2^i \,.$$

In Fig. 3-3, the obtained exact solution to the BDS equation and the exact analytic solution are illustrated for $Pe_m = 1$ and $b = 2$.

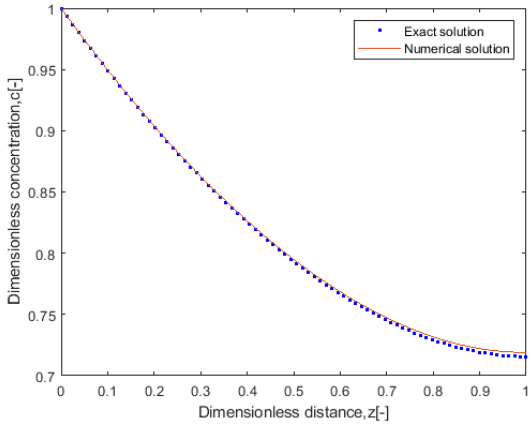

Figure 3-3: Dimensionless concentration profiles calculated by using explicit formula for the finite difference solution and analytic solution: $Pe_m = 1, b = 2, N = 80$.

3.3 Steady-state Equation with Power-law Kinetics

We consider the following one-component convection-diffusion-reaction equation

$$\frac{\partial^2 c}{\partial z^2} - Pe_m \frac{\partial c}{\partial z} - bc^p = 0, \tag{3.23}$$

where $p > 0$ is reaction exponent, b is the positive reaction rate constant. The non-linear differential equation is subject to the following boundary conditions

$$c = 1 \quad \text{at} \quad z = 0\,,$$

and

$$\frac{\partial c}{\partial z} = 0 \quad \text{at} \quad z = 1\,.$$

We apply the false transient method in order to find the steady-state solution. So, we consider the instationary equation

$$\frac{\partial c}{\partial t} = \frac{\partial^2 c}{\partial z^2} - Pe_m \frac{\partial c}{\partial z} - bc^p \tag{3.24}$$

subject to the initial condition

$$c(z, 0) = 1\,,$$

and boundary conditions

$$c(0,t) = 1\,,$$

$$\frac{\partial c}{\partial z}(1,t) = 0\,.$$

The Crank-Nicolson method [18] is applied to discretize this problem with respect to time, and we use the finite difference approximation in space. In this method, each term of the partial differential equation is transformed as follows

$$\begin{aligned}
\frac{\partial c}{\partial t} &\leftrightarrow \frac{c_j^{n+1} - c_j^n}{\Delta t}\,,\\
\frac{\partial^2 c}{\partial z^2} &\leftrightarrow \frac{1}{2}\left(\frac{c_{j-1}^{n+1} - 2c_j^{n+1} + c_{j+1}^{n+1}}{h^2} + \frac{c_{j-1}^{n} - 2c_j^{n} + c_{j+1}^{n}}{h^2}\right)\,,\\
\frac{\partial c}{\partial z} &\leftrightarrow \frac{1}{2}\left(\frac{c_j^{n+1} - c_{j-1}^{n+1}}{h} + \frac{c_j^{n} - c_{j-1}^{n}}{h}\right)\,,\\
c_j &\leftrightarrow \frac{1}{2}\left(c_j^{n+1} + c_j^n\right)\,.
\end{aligned} \tag{3.25}$$

Then, equations (3.25) are substituted into Eq. (3.23)

$$\begin{aligned}
\frac{c_j^{n+1} - c_j^n}{\Delta t} &= \frac{1}{2}\left(\frac{c_{j-1}^{n+1} - 2c_j^{n+1} + c_{j+1}^{n+1}}{h^2} + \frac{c_{j-1}^{n} - 2c_j^{n} + c_{j+1}^{n}}{h^2}\right)\\
&\quad - Pe_m\frac{1}{2}\left(\frac{c_j^{n+1} - c_{j-1}^{n+1}}{h} + \frac{c_j^{n} - c_{j-1}^{n}}{h}\right) - \frac{b}{2}\left((c_j^{n+1})^p + (c_j^n)^p\right)\\
&= \frac{1}{2h^2}c_{j+1}^{n+1} + \frac{1}{2}(-\frac{2}{h^2} - \frac{Pe}{h})c_j^{n+1} + \frac{1}{2}(\frac{1}{h^2} + \frac{Pe}{h})c_{j-1}^{n+1}\\
&\quad + \frac{1}{2h^2}c_{j+1}^{n} + \frac{1}{2}\left(-\frac{2}{h^2} - \frac{Pe}{h}\right)c_j^n + \frac{1}{2}\left(\frac{1}{h^2} + \frac{Pe}{h}\right)c_{j-1}^n\\
&\quad - \frac{b}{2}\left((c_j^{n+1})^p + (c_j^n)^p\right)\,.
\end{aligned} \tag{3.26}$$

The boundary conditions are applied when $j = 1$ and $j = N - 2$.

We have at $j = 1$ for new time terms $(n+1)$

$$\begin{aligned}
&\frac{1}{h^2}c_2^{n+1} + \left(-\frac{2}{h^2} - \frac{Pe_m}{h}\right)c_1^{n+1} + \left(\frac{1}{h^2} + \frac{Pe_m}{h}\right)c_0^{n+1}\\
&= \frac{1}{h^2}c_2^{n+1} + \left(-\frac{2}{h^2} - \frac{Pe_m}{h}\right)c_1^{n+1} + \left(\frac{1}{h^2} + \frac{Pe_m}{h}\right)\,,
\end{aligned}$$

and by analogy for the present time terms (n). There free constant is appeared which is the first entry of zero vector $\mathbf{f} = (f_1, \ldots, f_{N-2})^T \in \mathbb{R}^{N-2}$ and it is given by

$$f_1 = \left(\frac{2}{h^2} + \frac{2Pe}{h} \right) .$$

The second order approximation of the boundary boundary condition at $z = 1$, i.e., $\frac{c^n_{N-1} - c^n_{N-2}}{2h} = 0$ leads to the following difference equation at the grid point z_{N-2}

$$\begin{aligned} &\frac{1}{h^2} c^{n+1}_{N-1} + \left(-\frac{2}{h^2} - \frac{Pe}{h} \right) c^{n+1}_{N-2} + \left(\frac{1}{h^2} + \frac{Pe}{h} \right) c^{n+1}_{N-3} \\ &= \left(\frac{1}{h^2} - \frac{2}{h^2} - \frac{Pe}{h} \right) c^{n+1}_{N-2} + \left(\frac{1}{h^2} + \frac{Pe}{h} \right) c^{n+1}_{N-3} . \end{aligned}$$

Let us define

$$\mathbf{A} = \begin{pmatrix} \alpha & \beta & & & 0 \\ \gamma & \alpha & \beta & & \\ & \ddots & \ddots & \ddots & \\ & & \gamma & \alpha & \beta \\ 0 & & & \gamma & \alpha + \beta \end{pmatrix} ,$$

where

$$\alpha = -\frac{2}{h^2} - \frac{Pe}{h}; \quad \beta = \frac{1}{h^2}; \quad \gamma = \frac{1}{h^2} + \frac{Pe}{h} .$$

The difference equation (3.26) can be rewritten as nonlinear algebraic system

$$\frac{\mathbf{c}^{n+1} - \mathbf{c}^n}{\Delta t} = \frac{1}{2} \mathbf{A} \mathbf{c}^{n+1} + \frac{1}{2} \mathbf{A} \mathbf{c}^n - \frac{b}{2} \left((\mathbf{c}^{n+1})^p + (\mathbf{c}^n)^p \right) + \frac{1}{2} \mathbf{f} ,$$

where

$$\begin{aligned} \mathbf{c}^{n+1} &= (c^{n+1}_1, c^{n+1}_2, \ldots, c^{n+1}_{N-2})^T , \\ \mathbf{c}^n &= (c^n_1, c^n_2, \ldots, c^n_{N-2})^T , \\ \mathbf{f} &= (\frac{2}{h^2} + \frac{2Pe}{h}, 0, \ldots, 0)^T , \end{aligned}$$

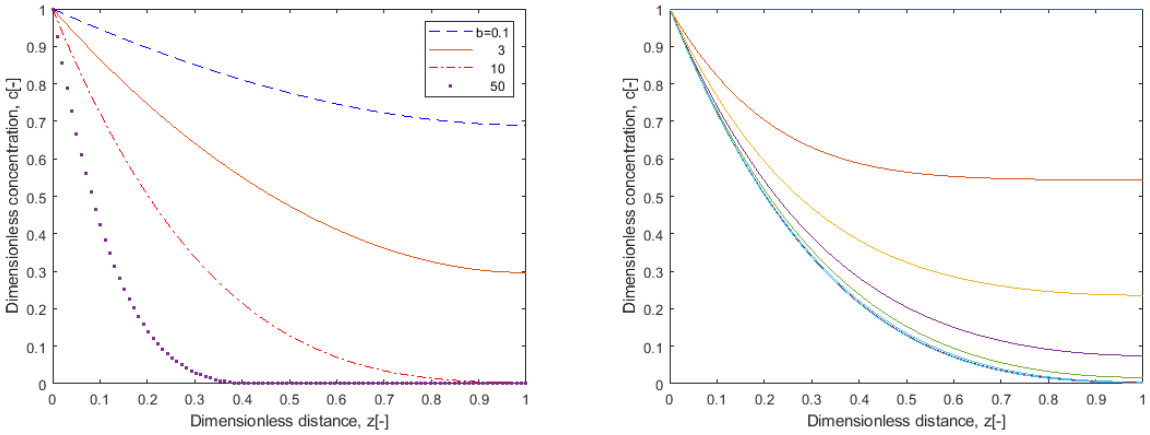

(a) Crank-Nicolson scheme

(b) Matlab *pdepe* solver [7]

Figure 3-4: Solutions for dead-core problem when $Pe_m = 1, p = 0.5$: (a) for different reaction rate constants $b = 0.1, 3, 10, 50$; (b) for reaction rate constant $b = 10$ and at the various times.

and we define

$$\mathbf{c}^p := ((\max\{c_1, 0\})^p, \ldots, (\max\{c_{N-2}, 0\})^p)^T$$

for $\mathbf{c} = (c_1, \ldots, c_{N-2})^T$. Consequently,

$$\mathbf{c}^{n+1} = \left(\mathbf{I} - \frac{1}{2}\Delta t\mathbf{A}\right)^{-1} \left\{\mathbf{c}^n + \frac{\Delta t}{2}\mathbf{A}\mathbf{c}^n - \frac{b\Delta t}{2}\left((\mathbf{c}^{n+1})^p + (\mathbf{c}^n)^p\right) + \frac{1}{2}\Delta t\mathbf{f}\right\}.$$

The concentration profile with dead-cores for different reaction constants $b = 0.1, 3, 10, 50$ are illustrated in Figure 3-4(a). Approximation of the dead-core solutions using pdepe Matlab solver [7] with $b = 10$ are shown in Fgure 3-4(b).

3.4 Steady-State Mass and Energy Balance Equations

In this section, the equations for the concentration of one component A and fot the temperature are considered. For the sake of simplicity we asterisk notation is omitted. The steady-state mass and energy balance equations are given by

$$\frac{\partial^2 c_A}{\partial z^2} - Pe_m\frac{\partial c_A}{\partial z} - \phi^2 \cdot e^{\gamma_1(1-\frac{1}{\theta})}c_A^p = 0\,,$$

$$\frac{\partial^2\theta}{\partial z^2} - Pe_h\frac{\partial\theta}{\partial z} - \beta_1 \cdot \phi^2 \cdot e^{\gamma_1(1-\frac{1}{\theta})}c_A^p = 0\,.$$

The dimensionless boundary conditions are given by the following equations.

At $z = 0$:

$$c_A = 1\,,$$
$$\theta = 1\,.$$

At $z = 1$:

$$\frac{\partial c_A}{\partial z} = 0\,,$$
$$\frac{\partial\theta}{\partial z} = 0\,.$$

Before we start computing solution to the above system, problem (3.1) is solved using the time-marching approach. The exact solution to the boundary value problem (3.1) is given by Eq.(3.10). Let us consider the instationary linear boundary value problem

$$\frac{\partial c}{\partial t} - \frac{\partial^2 c}{\partial z^2} + Pe_m\frac{\partial c}{\partial z} + bc = 0\,,$$
$$c(t,0) = 1\,,$$
$$c(0,t) = 1\,,$$
$$\frac{\partial c}{\partial z}(1,t) = 0\,,$$

where $b > 0$. Using the modified Crank-Nicolson scheme, the following difference equation is derived

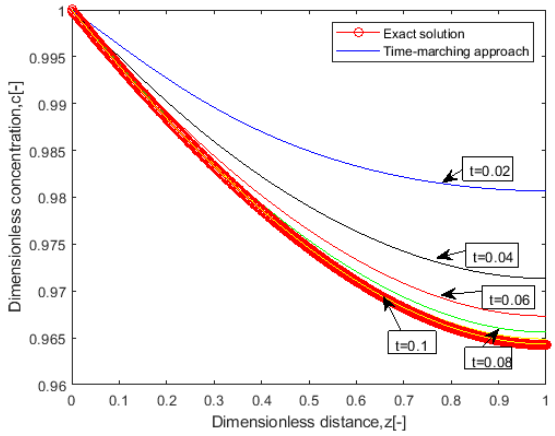

Figure 3-5: The concentration profiles $c(z,t)$ at various times $t = 0.02; 0.04; 0.06; 0.08; 0.1$.

$$\mathbf{c}^{n+1} = \left(\mathbf{I} - \frac{1}{2}\Delta t\mathbf{A}\right)^{-1} \left\{\mathbf{c}^n + \frac{1}{2}\Delta t\mathbf{A}\mathbf{c}^n - \Delta tb\mathbf{c}^n + \Delta t\mathbf{f}\right\}.$$

The numerical solution profiles at various times and the steady-state solution profile are shown in Fig. 3-5. The numerical solution tends exponentially fast to the exact steady-state solution when the time advances.

In the following, we will apply the time-marching method to approximate steady-state solutions to the nonlinear problems. The boundary value problem for the system of nonlinear differential equations can be solved by the technique from Section 3.3, which is based on the transient-false method. The steady-state equations are converted into unsteady-state partial differential equations and solved numerically by Crank-Nicolson method.

The transient system of partial differential equations is given as follows

$$\begin{aligned} \frac{\partial c_A}{\partial t} &= \frac{\partial^2 c_A}{\partial z^2} - Pe_m\frac{\partial c_A}{\partial z} - \phi^2 exp\left(\gamma_1(1-\frac{1}{\theta})\right)c_A^p\,, \\ \frac{\partial \theta}{\partial t} &= \frac{\partial^2 \theta}{\partial z^2} - Pe_h\frac{\partial \theta}{\partial z} - \beta_1\phi^2 exp\left(\gamma_1(1-\frac{1}{\theta})\right)c_A^p\,. \end{aligned} \tag{3.27}$$

The initial conditions are prescribed as

$$\begin{aligned} c_A(z,t_0) &= c_{A0}\,, \\ \theta(z,t_0) &= \theta_0\,, \end{aligned}$$

where c_{A0} and θ_0 are the initial concentration and temperature.

The boundary conditions in the dimensionless form are given as

$$\begin{aligned} c_A(0,t) &= 1\,, \\ \theta(0,t) &= 1\,, \end{aligned}$$

$$\begin{aligned} \frac{\partial c_A}{\partial z}|_{z=1} &= 0\,, \\ \frac{\partial \theta}{\partial z}|_{z=1} &= 0\,. \end{aligned}$$

Then, we discretize the system by the Crank-Nicolson method, and the system can

be written as

$$\begin{aligned}
\frac{c_{A,j}^{n+1}-c_{A,j}^{n}}{\Delta t} &= \frac{1}{2}\left(\frac{c_{A,j-1}^{n+1}-2c_{A,j}^{n+1}+c_{A,j+1}^{n+1}}{h^2}+\frac{c_{A,j-1}^{n}-2c_{A,j}^{n}+c_{A,j+1}^{n}}{h^2}\right)\\
&\quad - Pe_m\frac{1}{2}\left(\frac{c_{A,j}^{n+1}-c_{A,j-1}^{n+1}}{h}+\frac{c_{A,j}^{n}-c_{A,j-1}^{n}}{h}\right)\\
&\quad - \frac{1}{2}\phi^2 exp\left(\gamma_1(1-\frac{1}{\theta})\right)\left((c_{A,j}^{n})^p+(c_{A,j}^{n+1})^p\right)\,,\\
\frac{\theta_{j}^{n+1}-\theta_{j}^{n}}{\Delta t} &= \frac{1}{2}\left(\frac{\theta_{j-1}^{n+1}-2\theta_{j}^{n+1}+\theta_{j+1}^{n+1}}{h^2}+\frac{\theta_{j-1}^{n}-2\theta_{j}^{n}+\theta_{j+1}^{n}}{h^2}\right)\\
&\quad - Pe_h\frac{1}{2}\left(\frac{\theta_{j}^{n+1}-\theta_{j-1}^{n+1}}{h}+\frac{\theta_{j}^{n}-\theta_{j-1}^{n}}{h}\right)\\
&\quad - \frac{1}{2}\beta_1\phi^2\left(exp\left(\gamma_1(1-\frac{1}{\theta_j^n})\right)+exp\left(\gamma_1(1-\frac{1}{\theta_j^{n+1}})\right)\right)(c_{A,j}^{n})^p\,.
\end{aligned}$$

Addition of like-terms on the right-hand side of above equations results in

$$\begin{aligned}
\frac{c_{A,j}^{n+1}-c_{A,j}^{n}}{\Delta t} &= \frac{1}{2h^2}c_{A,j+1}^{n+1}+\frac{1}{2}\left(-\frac{2}{h^2}-\frac{Pe}{h}\right)c_{A,j}^{n+1}+\frac{1}{2}\left(\frac{1}{h^2}+\frac{Pe}{h}\right)c_{A,j-1}^{n+1}\\
&\quad + \frac{1}{2h^2}c_{A,j+1}^{n}+\frac{1}{2}\left(-\frac{2}{h^2}-\frac{Pe}{h}\right)c_{A,j}^{n}+\frac{1}{2}\left(\frac{1}{h^2}+\frac{Pe}{h}\right)c_{A,j-1}^{n}\\
&\quad - \frac{1}{2}\phi^2 exp\left(\gamma_1(1-\frac{1}{\theta})\right)\left((c_{A,j}^{n})^p+(c_{A,j}^{n+1})^p\right)\,,
\end{aligned}\tag{3.28}$$

$$\begin{aligned}
\frac{\theta_{j}^{n+1}-\theta_{j}^{n}}{\Delta t} &= \frac{1}{2h^2}\theta_{j+1}^{n+1}+\frac{1}{2}\left(-\frac{2}{h^2}-\frac{Pe_h}{h}\right)\theta_{j}^{n+1}+\frac{1}{2}\left(\frac{1}{h^2}+\frac{Pe_h}{h}\right)\theta_{j-1}^{n+1}\\
&\quad + \frac{1}{2h^2}\theta_{j+1}^{n}+\frac{1}{2}\left(-\frac{2}{h^2}-\frac{Pe_h}{h}\right)\theta_{j}^{n}+\frac{1}{2}\left(\frac{1}{h^2}+\frac{Pe_h}{h}\right)\theta_{j-1}^{n}\\
&\quad - \frac{1}{2}\beta_1\phi^2\left(exp\left(\gamma_1(1-\frac{1}{\theta_j^{n+1}})\right)+exp\left(\gamma_1(1-\frac{1}{\theta_j^n})\right)\right)(c_{A,j}^{n})^p\,.
\end{aligned}\tag{3.29}$$

The boundary conditions are written as

$$c_A^n(0,t)=1\,,$$

$$\theta^n(0,t)=1\,,$$

$$\frac{\partial c_A}{\partial z}|_{z=1} = \frac{c^n_{A,N-1} - c^n_{A,N-2}}{2h} = 0\,,$$
$$\frac{\partial \theta}{\partial z}|_{z=1} = \frac{\theta^n_{N-1} - \theta^n_{N-2}}{2h} = 0\,.$$

Taking into account the boundary conditions, Eqs. (3.28) and (3.29) can be expressed in the matrix form

$$\frac{\mathbf{c}^{n+1}_A - \mathbf{c}^n_A}{\Delta t} = \frac{1}{2}\mathbf{A}\mathbf{c}^{n+1}_A + \frac{1}{2}\mathbf{A}\mathbf{c}^n_A - \frac{1}{2}\phi^2 \mathbf{exp}\left(\gamma_1(1-\frac{1}{\theta})\right)\left((C^n_{A,j})^p + (C^{n+1}_{A,j})^p\right) + \frac{1}{2}\mathbf{f}_A\,,$$

$$\begin{aligned}\frac{\boldsymbol{\theta}^{n+1} - \boldsymbol{\theta}^n}{\Delta t} = &\frac{1}{2}\mathbf{B}\boldsymbol{\theta}^{n+1} + \frac{1}{2}\mathbf{B}\boldsymbol{\theta}^n \\ &- \frac{1}{2}\beta_1\phi^2\left(\mathbf{exp}\left(\gamma_1(1-\frac{1}{\boldsymbol{\theta}^n})\right) + \mathbf{exp}\left(\gamma_1(1-\frac{1}{\boldsymbol{\theta}^{n+1}})\right)\right)(\mathbf{c}^n_A)^p + \frac{1}{2}\mathbf{f}_\theta\,,\end{aligned}$$

where $\mathbf{A}$ and $\mathbf{B}$ are matrices with size $N-2$

$$\mathbf{A} = \begin{pmatrix} \alpha & \beta & & & 0 \\ \gamma & \ddots & \ddots & & \\ & \ddots & \ddots & \ddots & \\ & & \gamma & \alpha & \beta \\ 0 & & & \gamma & \alpha+\beta \end{pmatrix}, \quad \mathbf{B} = \begin{pmatrix} \kappa & \beta & & & 0 \\ \mu & \ddots & \ddots & & \\ & \ddots & \ddots & \ddots & \\ & & \mu & \kappa & \beta \\ 0 & & & \mu & \kappa+\beta \end{pmatrix} \tag{3.30}$$

with the following entries

$$\alpha = -\frac{2}{h^2} - \frac{Pe_m}{h}; \quad \beta = \frac{1}{h^2}; \quad \gamma = \frac{1}{h^2} + \frac{Pe_m}{h}\,, \tag{3.31}$$

$$\kappa = -\frac{2}{h^2} - \frac{Pe_h}{h}; \quad \beta = \frac{1}{h^2}; \quad \mu = \frac{1}{h^2} + \frac{Pe_h}{h}\,. \tag{3.32}$$

Here, we use the followig notations

$$\mathbf{c}^{n+1}_A = \begin{pmatrix} c^{n+1}_{A,1} \\ c^{n+1}_{A,2} \\ \vdots \\ c^{n+1}_{A,N-2} \end{pmatrix}, \quad \mathbf{c}^n_A = \begin{pmatrix} c^n_{A,1} \\ c^n_{A,2} \\ \vdots \\ c^n_{A,N-2} \end{pmatrix}, \quad \mathbf{f}_A = \begin{pmatrix} \frac{2}{h^2} + \frac{2Pe_m}{h} \\ 0 \\ \vdots \\ 0 \end{pmatrix}, \tag{3.33}$$

$$\boldsymbol{\theta}^{n+1} = \begin{pmatrix} \theta_1^{n+1} \\ \theta_2^{n+1} \\ \vdots \\ \theta_{N-2}^{n+1} \end{pmatrix}, \quad \boldsymbol{\theta}^{n} = \begin{pmatrix} \theta_1^{n} \\ \theta_2^{n} \\ \vdots \\ \theta_{N-2}^{n} \end{pmatrix}, \quad \mathbf{f}_\theta = \begin{pmatrix} \frac{2}{h^2} + \frac{2Pe_h}{h} \\ 0 \\ \vdots \\ 0 \end{pmatrix}, \tag{3.34}$$

and set

$$\mathbf{exp}\left(\gamma_1(1-\frac{1}{\boldsymbol{\theta}^n})\right) := \begin{pmatrix} exp\left(\gamma_1(1-\frac{1}{\theta_1^n})\right) \\ exp\left(\gamma_1(1-\frac{1}{\theta_2^n})\right) \\ \vdots \\ exp\left(\gamma_1(1-\frac{1}{\theta_{N-2}^n})\right) \end{pmatrix}.$$

Rearranging the term, we obtain the following system of nonlinear algebraic equations for the unknwon vectors $\mathbf{c}_A^{n+1}$ and $\boldsymbol{\theta}^{n+1}$

$$\begin{aligned} \mathbf{c}_A^{n+1} = \left(\mathbf{I} - \frac{1}{2}\Delta t\mathbf{A}\right)^{-1} \Big\{ & \mathbf{c}_A^n + \frac{1}{2}\Delta t\mathbf{A}\mathbf{c}_A^n - \\ & - \frac{1}{2}\Delta t\phi^2 \mathbf{exp}\left(\gamma_1(1-\frac{1}{\boldsymbol{\theta}^n})\right)\left((\mathbf{c}_A^n)^p + (\mathbf{c}_A^{n+1})^p\right) \\ & + \frac{1}{2}\Delta t\mathbf{f}_A \Big\}, \\ \boldsymbol{\theta}^{n+1} = \left(\mathbf{I} - \frac{1}{2}\Delta t\mathbf{A}\right)^{-1} \Big\{ & \boldsymbol{\theta}^n + \frac{1}{2}\Delta t\mathbf{A}\boldsymbol{\theta}^n \\ & - \frac{1}{2}\Delta t\beta_1\phi^2 \left(\mathbf{exp}\left(\gamma_1(1-\frac{1}{\boldsymbol{\theta}^n})\right) + \mathbf{exp}\left(\gamma_1(1-\frac{1}{\boldsymbol{\theta}^{n+1}})\right)\right)(\mathbf{c}_A^n)^p \\ & + \frac{1}{2}\Delta t f_\theta \Big\}. \end{aligned}$$

The solution in each time step can be obtained numerically using fixed-point iteration and the direct Matlab solver for linear systems [7]. Fig. 3-6 and Fig. 3-7 illustrate the concentration profiles for dead-core problem with temperature-dependent diffusion coefficient.

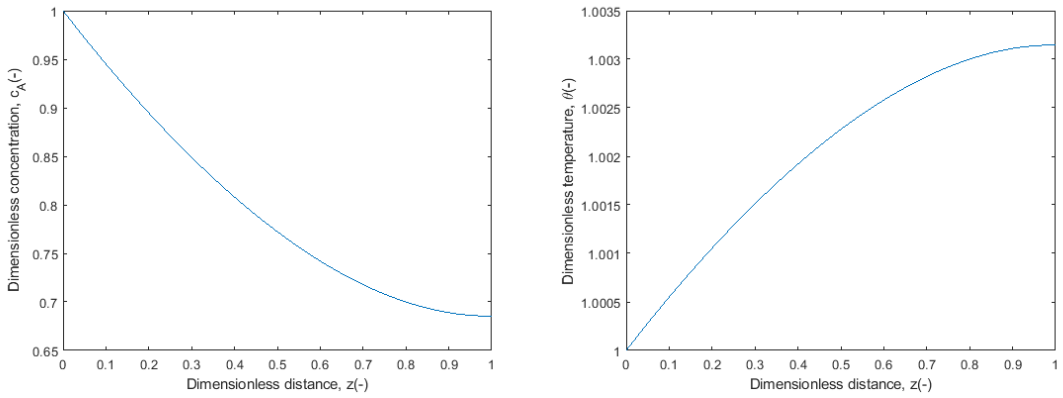

(a) (b)

Figure 3-6: Solutions for concentration and temperature when without dead-core for $Pe_m = 1, Pe_h = 1, p = 0.5, \phi = 0.5, \beta_1 = 0.01$

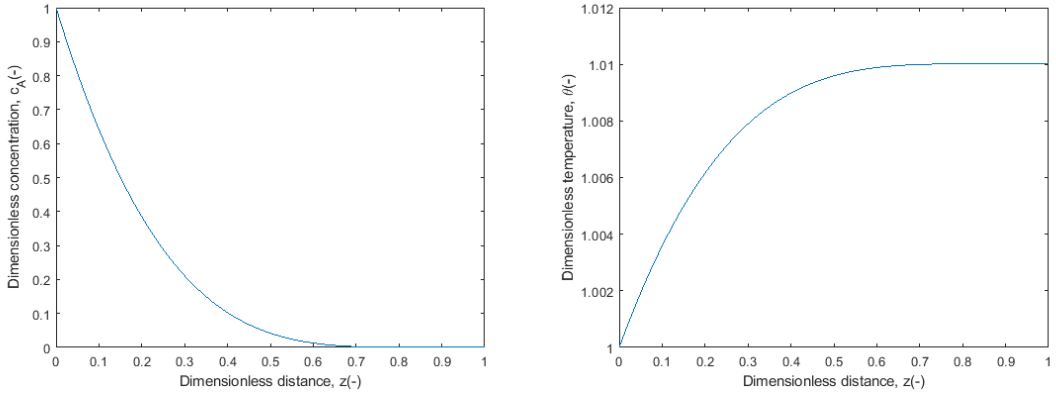

(a) (b)

Figure 3-7: Solutions with dead-core problem concentration and temperature when $Pe_m = 1, Pe_h = 1, p = 0.5, \phi = 2, \beta_1 = 0.01$

3.5 The Full System

The full system includes mass balance equations for both components A,B and energy balance equation. The system of nonlinear differential equations for our model reads

as follows

$$\begin{aligned}
\frac{\partial^2 c_A^*}{\partial z^2} - Pe_m \frac{\partial c_A^*}{\partial z} - \phi^2 \frac{\xi}{\psi} exp\left(\gamma_1(1-\frac{1}{\theta})\right) c_A^{*p} = 0\,, \\
\frac{\partial^2 c_B^*}{\partial z^2} - Pe_m \psi \frac{\partial c_B^*}{\partial z} - \phi^2 exp\left(\gamma_2(1-\frac{1}{\theta})\right) c_B^{*p} + \phi^2 \xi exp\left(\gamma_1(1-\frac{1}{\theta})\right) c_A^{*p} = 0\,, \\
\frac{\partial^2 \theta}{\partial z^2} - Pe_h \frac{\partial \theta}{\partial z} + \beta_1 \phi^2 \frac{\xi}{\psi} exp\left(\gamma_1(1-\frac{1}{\theta})\right) c_A^{*p} + \beta_2 \phi^2 exp\left(\gamma_2(1-\frac{1}{\theta})\right) c_B^{*p} = 0\,.
\end{aligned} \tag{3.35}$$

The boundary conditions at $z = 0$ is given by

$$c_A^* = 1\,, \quad c_B^* = 0\,, \quad \theta = 1\,,$$

whereas the boundary conditions at $z = 1$ are

$$\frac{\partial c_A^*}{\partial z} = 0\,, \quad \frac{\partial c_A^*}{\partial z} = 0\,, \quad \frac{\partial \theta}{\partial z} = 0\,.$$

Now we add mass balance equation of component B to the unsteady-state system Eq.(3.27), and get the following

$$\begin{aligned}
\frac{\partial c_A^*}{\partial t} &= \frac{\partial^2 c_A^*}{\partial z^2} - Pe_m \frac{\partial c_A^*}{\partial z} - \phi^2 \frac{\xi}{\psi} exp\left(\gamma_1(1-\frac{1}{\theta})\right) c_A^{*p}\,, \\
\frac{\partial c_B^*}{\partial t} &= \frac{\partial^2 c_B^*}{\partial z^2} - Pe_m \psi \frac{\partial c_B^*}{\partial z} - \phi^2 exp\left(\gamma_2(1-\frac{1}{\theta})\right) c_B^{*p} + \phi^2 \xi exp\left(\gamma_1(1-\frac{1}{\theta})\right) c_A^{*p}\,, \\
\frac{\partial \theta}{\partial t} &= \frac{\partial^2 \theta}{\partial z^2} - Pe_h \frac{\partial \theta}{\partial z} + \beta_1 \phi^2 \frac{\xi}{\psi} exp\left(\gamma_1(1-\frac{1}{\theta})\right) c_A^{*p} + \beta_2 \phi^2 exp\left(\gamma_2(1-\frac{1}{\theta})\right) c_B^{*p}
\end{aligned}$$

subject to the boundary conditions and initial conditions

$$\begin{aligned}
c_A^*(z,0) &= c_{A0}^*\,, \\
c_B^*(z,0) &= c_{B0}^*\,, \\
\theta(z,0) &= \theta_0\,,
\end{aligned}$$

where c_{A0}^*, c_{B0}^* and θ_0 are the initial concentrations for A, B, and the initial temperature, respectively.

Applying Crank-Nicolson method, yields

$$
\begin{aligned}
&\frac{c_{A,j}^{*,n+1}-c_{A,j}^{*,n}}{\Delta t}\\
&=\frac{1}{2h^2}c_{A,j+1}^{*,n+1}+\frac{1}{2}\left(-\frac{2}{h^2}-\frac{Pe}{h}\right)c_{A,j}^{*,n+1}+\frac{1}{2}\left(\frac{1}{h^2}+\frac{Pe}{h}\right)c_{A,j-1}^{*,n+1}\\
&\quad+\frac{1}{2h^2}c_{A,j+1}^{*,n}+\frac{1}{2}\left(-\frac{2}{h^2}-\frac{Pe}{h}\right)c_{A,j}^{*,n}+\frac{1}{2}\left(\frac{1}{h^2}+\frac{Pe}{h}\right)c_{A,j-1}^{*,n}\\
&\quad-\frac{1}{2}\phi^2\frac{\xi}{\psi}exp\left(\gamma_1(1-\frac{1}{\theta_j^n})\right)\left((c_{A,j}^{*n})^p+(c_{A,j}^{*n+1})^p\right),\\
&\frac{c_{B,j}^{*n+1}-c_{B,j}^{*n}}{\Delta t}\\
&=\frac{1}{2h^2}c_{B,j+1}^{*n+1}+\frac{1}{2}\left(-\frac{2}{h^2}-\frac{\psi Pe_m}{h}\right)c_{B,j}^{*n+1}+\frac{1}{2}\left(\frac{1}{h^2}+\frac{\psi Pe_m}{h}\right)c_{B,j-1}^{*n+1}\\
&\quad+\frac{1}{2h^2}c_{B,j+1}^{*n}+\frac{1}{2}\left(-\frac{2}{h^2}-\frac{\psi Pe_m}{h}\right)c_{B,j}^{*n}+\frac{1}{2}\left(\frac{1}{h^2}+\frac{\psi Pe_m}{h}\right)c_{B,j-1}^{*n}\\
&\quad+\phi^2\frac{\xi}{\psi}exp\left(\gamma_1(1-\frac{1}{\theta_j^n})\right)(c_{A,j}^{*n})^p\\
&\quad-\frac{1}{2}\phi^2 exp\left(\gamma_2(1-\frac{1}{\theta_j^n})\right)\left((c_{B,j}^{*n})^p+(c_{B,j}^{*n+1})^p\right),\\
&\frac{\theta_j^{n+1}-\theta_j^n}{\Delta t}\\
&=\frac{1}{2h^2}\theta_{j+1}^{n+1}+\frac{1}{2}\left(-\frac{2}{h^2}-\frac{Pe_h}{h}\right)\theta_j^{n+1}+\frac{1}{2}\left(\frac{1}{h^2}+\frac{Pe_h}{h}\right)\theta_{j-1}^{n+1}\\
&\quad+\frac{1}{2h^2}\theta_{j+1}^{n}+\frac{1}{2}\left(-\frac{2}{h^2}-\frac{Pe_h}{h}\right)\theta_j^{n}+\frac{1}{2}\left(\frac{1}{h^2}+\frac{Pe_h}{h}\right)\theta_{j-1}^{n}\\
&\quad+\frac{1}{2}\beta_1\phi^2\frac{\xi}{\psi}\left(exp\left(\gamma_1(1-\frac{1}{\theta_j^n})\right)+exp\left(\gamma_1(1-\frac{1}{\theta_j^{n+1}})\right)\right)*(c_{A,j}^{*n})^p\\
&\quad+\frac{1}{2}\beta_2\phi^2\left(exp\left(\gamma_2(1-\frac{1}{\theta_j^n})\right)+exp\left(\gamma_2(1-\frac{1}{\theta_j^{n+1}})\right)\right)(c_{B,j}^{*n})^p.
\end{aligned}
\tag{3.36}
$$

The boundary conditions are specified as follows

$$
\begin{aligned}
c_A^{*n}(0,t)&=1,\\
c_B^{*n}(0,t)&=0,\\
\theta^n(0,t)&=1,
\end{aligned}
\tag{3.37}
$$

$$
\begin{aligned}
\frac{\partial c_A^*}{\partial z}\Big|_{z=1} &\approx \frac{c_{A,N-1}^{*n} - c_{A,N-2}^{*n}}{2h} = 0\,, \\
\frac{\partial c_B^*}{\partial z}\Big|_{z=1} &\approx \frac{c_{B,N-1}^{*n} - c_{B,N-2}^{*n}}{2h} = 0\,, \\
\frac{\partial \theta}{\partial z}\Big|_{z=1} &\approx \frac{\theta_{N-1}^{n} - \theta_{N-2}^{n}}{2h} = 0\,.
\end{aligned}
\tag{3.38}
$$

From Eq. (3.36) with boundary conditions Eq. (3.37), Eq. (3.38) we get the equations in matrix form

$$
\begin{aligned}
&\frac{\mathbf{c}_A^{n+1} - \mathbf{c}_A^n}{\Delta t} \\
&= \frac{1}{2}\mathbf{A}\mathbf{c}_A^{n+1} + \frac{1}{2}\mathbf{A}\mathbf{c}_A^n - \frac{1}{2}\phi^2\frac{\xi}{\psi}\mathbf{exp}\left(\gamma_1(1-\frac{1}{\boldsymbol{\theta}^n})\right)\left((\mathbf{c}_A^n)^p + (\mathbf{c}_A^{n+1})^p\right) + \frac{1}{2}\mathbf{f}_A\,, \\
&\frac{\mathbf{c}_B^{n+1} - \mathbf{c}_B^n}{\Delta t} \\
&= \frac{1}{2}\mathbf{M}\mathbf{c}_B^{n+1} + \frac{1}{2}\mathbf{M}\mathbf{c}_B^n + \phi^2\frac{\xi}{\psi}\mathbf{exp}\left(\gamma_1(1-\frac{1}{\boldsymbol{\theta}^n})\right)(\mathbf{c}_A^n)^p \\
&\quad - \frac{1}{2}\phi^2\mathbf{exp}\left(\gamma_2(1-\frac{1}{\boldsymbol{\theta}^n})\right)\left((\mathbf{c}_B^n)^p + (\mathbf{c}_B^{n+1})^p\right) + \frac{1}{2}\mathbf{f}_B\,, \\
&\frac{\boldsymbol{\theta}^{n+1} - \boldsymbol{\theta}^n}{\Delta t} \\
&= \frac{1}{2}\mathbf{A}\boldsymbol{\theta}^{n+1} + \frac{1}{2}\mathbf{A}\boldsymbol{\theta}^n \\
&\quad + \frac{1}{2}\beta_1\phi^2\frac{\xi}{\psi}\left(\mathbf{exp}\left(\gamma_1(1-\frac{1}{\boldsymbol{\theta}^n})\right) + \mathbf{exp}\left(\gamma_1(1-\frac{1}{\boldsymbol{\theta}^{n+1}})\right)\right)(\mathbf{c}_A^n)^p \\
&\quad + \frac{1}{2}\beta_2\phi^2\left(\mathbf{exp}\left(\gamma_2(1-\frac{1}{\boldsymbol{\theta}^n})\right) + \mathbf{exp}\left(\gamma_2(1-\frac{1}{\boldsymbol{\theta}^{n+1}})\right)\right)(\mathbf{c}_B^n)^p + \frac{1}{2}\mathbf{f}_\theta\,,
\end{aligned}
\tag{3.39}
$$

where $\mathbf{A}$ and $\mathbf{B}$ are matrices from the previous Sec.(3.4) (Eq. (3.30) with the Eq.(3.31) and Eq. (3.32) for coefficients). Also, the vectors for $\mathbf{c}_A^n$, $\mathbf{c}_A^{n+1}$, $\mathbf{f}_A$, $\boldsymbol{\theta}$, and for $\mathbf{f}_\theta$ are equal to vectors from Equations (3.33) and (3.34). The vectors $\mathbf{c}_B^n$, $\mathbf{c}_B^{n+1}$, $\mathbf{f}_B$ and the

matrix $\mathbf{M} \in \mathbb{R}^{(N-2)\times(N-2)}$ are given by

$$\mathbf{c}_B^{n+1} = \begin{pmatrix} c_{B,1}^{*n+1} \\ c_{B,2}^{*n+1} \\ \vdots \\ c_{B,N-2}^{*n+1} \end{pmatrix}, \quad \mathbf{c}_B^{n} = \begin{pmatrix} c_{B,1}^{*n} \\ c_{B,2}^{*n} \\ \vdots \\ c_{B,N-2}^{*n} \end{pmatrix}, \quad \mathbf{f}_B = \begin{pmatrix} \frac{2}{h^2} + \frac{2\psi Pe_m}{h} \\ 0 \\ \vdots \\ 0 \end{pmatrix}$$

and

$$\mathbf{M} = \begin{pmatrix} m & \beta & & & 0 \\ l & \ddots & \ddots & & \\ & \ddots & \ddots & \ddots & \\ & & l & m & \beta \\ 0 & & & l & m+\beta \end{pmatrix},$$

where

$$m = -\frac{2}{h^2} - \frac{\psi Pe_m}{h}; \quad \beta = \frac{1}{h^2}; \quad l = \frac{1}{h^2} + \frac{\psi Pe_m}{h},$$

respectively. Consequenty, the algebraic systems for $\mathbf{c}_A^{n+1}$, $\mathbf{c}_B^{n+1}$, $\boldsymbol{\theta}^{n+1}$ are given as

$$\begin{aligned} \mathbf{c}_A^{n+1} = \left(\mathbf{I} - \frac{1}{2}\Delta t\mathbf{A}\right)^{-1} \Big\{ & \mathbf{c}_A^n + \frac{1}{2}\Delta t\mathbf{A}\mathbf{c}_A^n \\ & - \frac{1}{2}\Delta t\phi^2 \frac{\xi}{\psi}\mathbf{exp}\left(\gamma_1(1 - \frac{1}{\boldsymbol{\theta}^n})\right)\left((\mathbf{c}_A^n)^p + (\mathbf{c}_A^{n+1})^p\right) \\ & + \frac{1}{2}\Delta t\mathbf{f}_A \Big\}, \end{aligned}$$

$$\begin{aligned} \mathbf{c}_B^{n+1} = \left(\mathbf{I} - \frac{1}{2}\Delta t\mathbf{M}\right)^{-1} \Big\{ & \mathbf{c}_B^n + \frac{1}{2}\Delta t\mathbf{M}\mathbf{c}_B^n \\ & + \Delta t\phi^2 \frac{\xi}{\psi}\mathbf{exp}\left(\gamma_1(1 - \frac{1}{\boldsymbol{\theta}^n})\right)(\mathbf{c}_A^n)^p \\ & - \frac{1}{2}\Delta t\phi^2\mathbf{exp}\left(\gamma_2(1 - \frac{1}{\boldsymbol{\theta}^n})\right)\left((\mathbf{c}_B^n)^p + (\mathbf{c}_B^{n+1})^p\right) \\ & + \frac{1}{2}\Delta t\mathbf{f}_B) \Big\}, \end{aligned}$$

$$\boldsymbol{\theta}^{n+1} = \left(\mathbf{I} - \frac{1}{2}\Delta t\mathbf{A}\right)^{-1}\Big\{\boldsymbol{\theta}^n + \frac{1}{2}\Delta t\mathbf{A}\boldsymbol{\theta}^n$$
$$+ \frac{1}{2}\Delta t\beta_1\phi^2\frac{\xi}{\psi}\left(\mathbf{exp}\left(\gamma_1(1-\frac{1}{\boldsymbol{\theta}^n})\right) + \mathbf{exp}\left(\gamma_1(1-\frac{1}{\boldsymbol{\theta}^{n+1}})\right)\right)(\mathbf{c}_A^n)^p$$
$$+ \frac{1}{2}\Delta t\beta_2\phi^2\left(\mathbf{exp}\left(\gamma_2(1-\frac{1}{\boldsymbol{\theta}^n})\right) + \mathbf{exp}\left(\gamma_2(1-\frac{1}{\boldsymbol{\theta}^{n+1}})\right)\right)(\mathbf{c}_B^n)^p$$
$$+ \frac{1}{2}\Delta t\mathbf{f}_\theta\Big\}.$$

In each time step, the nonlinear algebraic systems are solved approximately using the fixed point iterations where the linear sparse systems are solved exact using the direct *backslash* Matlab solver [7]. In the next Chapter, numerical results will be provided.

Chapter 4

Numerical Results and Discussion

In the previous chapter, the full system of equations subject to the boundary conditions were solved using the Crank-Nicolson method. The results were verified using the analytic solutions and *pdepe* Matlab solver [7]. Further sections show the results of the full system.

In our model, ten process parameters were used. They could have effects on the overall performance indicators. In the present study the effects of several parameters, such as Pe_m, Pe_h, ϕ, p, are mainly investigated. Therefore, other parameters were considered as constants, namely $\psi = 1, \xi = 4, \gamma_1 = 10, \gamma_2 = 20, \beta_1 = \beta_2 = 0.01$. [6]

4.1 Solution Profiles

4.1.1 Effects of Mass Peclet and Heat Peclet Numbers

The mass and heat Peclet numbers are the dimensionless groups which describe the effect on convection. [13]

The variations of concentration with respect to Pe_m and Pe_h are shown in Fig. 4-1 and Fig. 4-2, respectively. The concentration profile with Pe_m simulated for the following model parameters: $Pe_h = 1, p = 0.5$ and $\phi = 2.2$. The choice of the reaction order p and Thiele modulus ϕ were accordig to the conditions for the existence of the dead zone.

Andreev [5] investigated the necessary conditions for the formation of the dead-zones in porous media and materials. The results of his work can be applied to our model with the power-law kinetics and irreversible consecutive reaction. Thus, for the formation of the dead-zone, necessary condition should be $|p| < 1$, and for the sufficient condition $\phi \geq \phi^*$, where ϕ^* is a critical Thiele modulus which can be estimated in the case of one component model by analogy to the paper of Andreev, Skrzypacz, and Golman [12]. They derived critical Thiele modulus for the temperature-dependent diffusion-reaction with power-law kinetics.

In Fig. 4-1 and Fig. 4-2 the convective flow is assumed to be in the positive z-

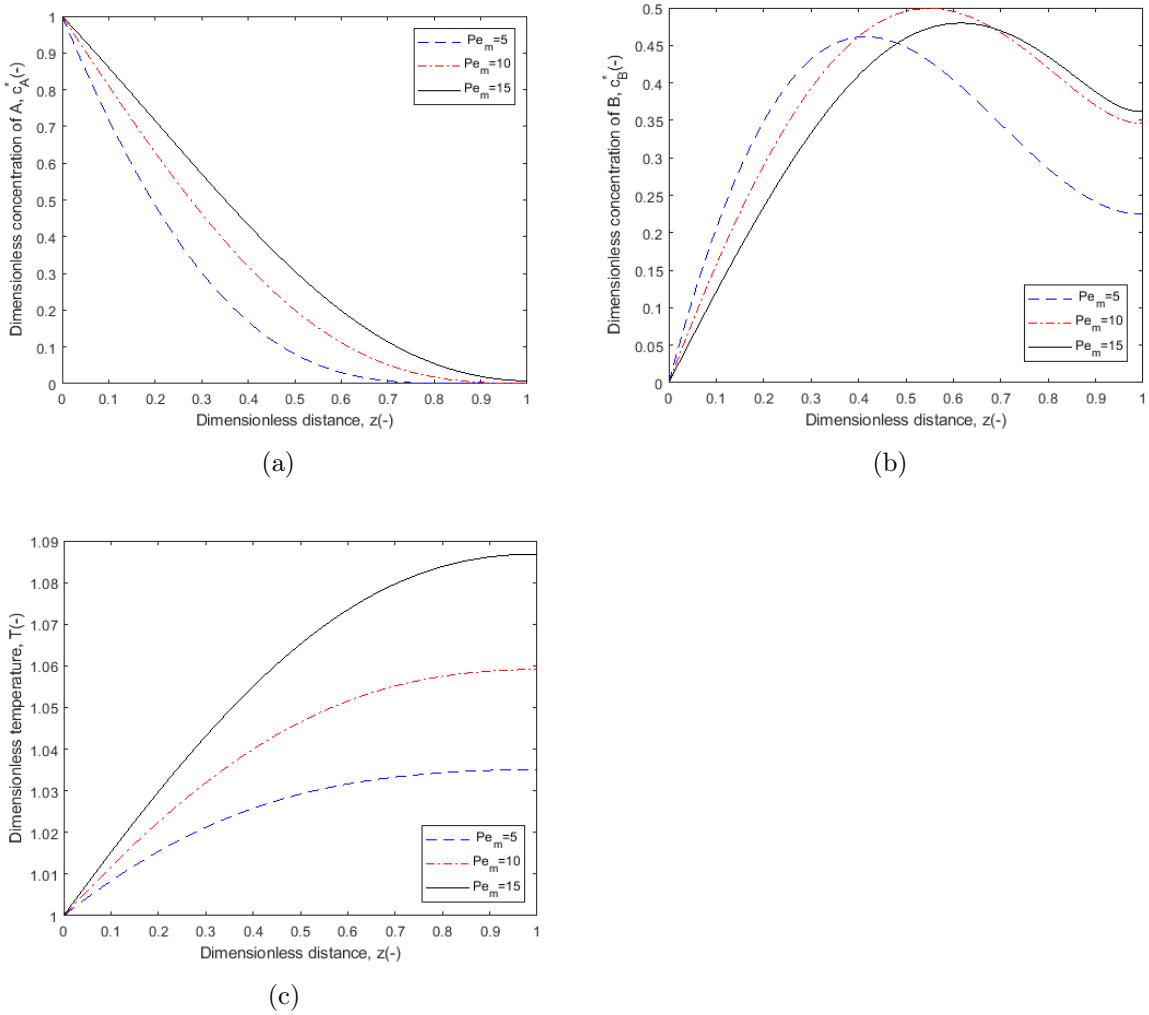

Figure 4-1: Solution profiles simulated for model parameters $Pe_h = 1, p = 0.5, \phi = 2.2$.

direction.. Fig. 4-1(a) describes dimensionless concentration profile of reactant A. In Fig. 4-1(a) as the mass Peclet numbers $Pe_m = 5, 10, 15$ decreases the corresponding graph of concentration goes down sharply. The concentration profile with lower values of Peclet number exhibit the dead zones. However, for the highest $Pe_m = 15$ concentration profile does not exhibit a dead zone. Also, it can be seen that the dead zone length increases with a decrease in the Peclet number. The low value of Peclet number makes diffusion dominating over convection. High rate flow can cause an increase in concentration of reactants which may lead to the high productivity. [14]

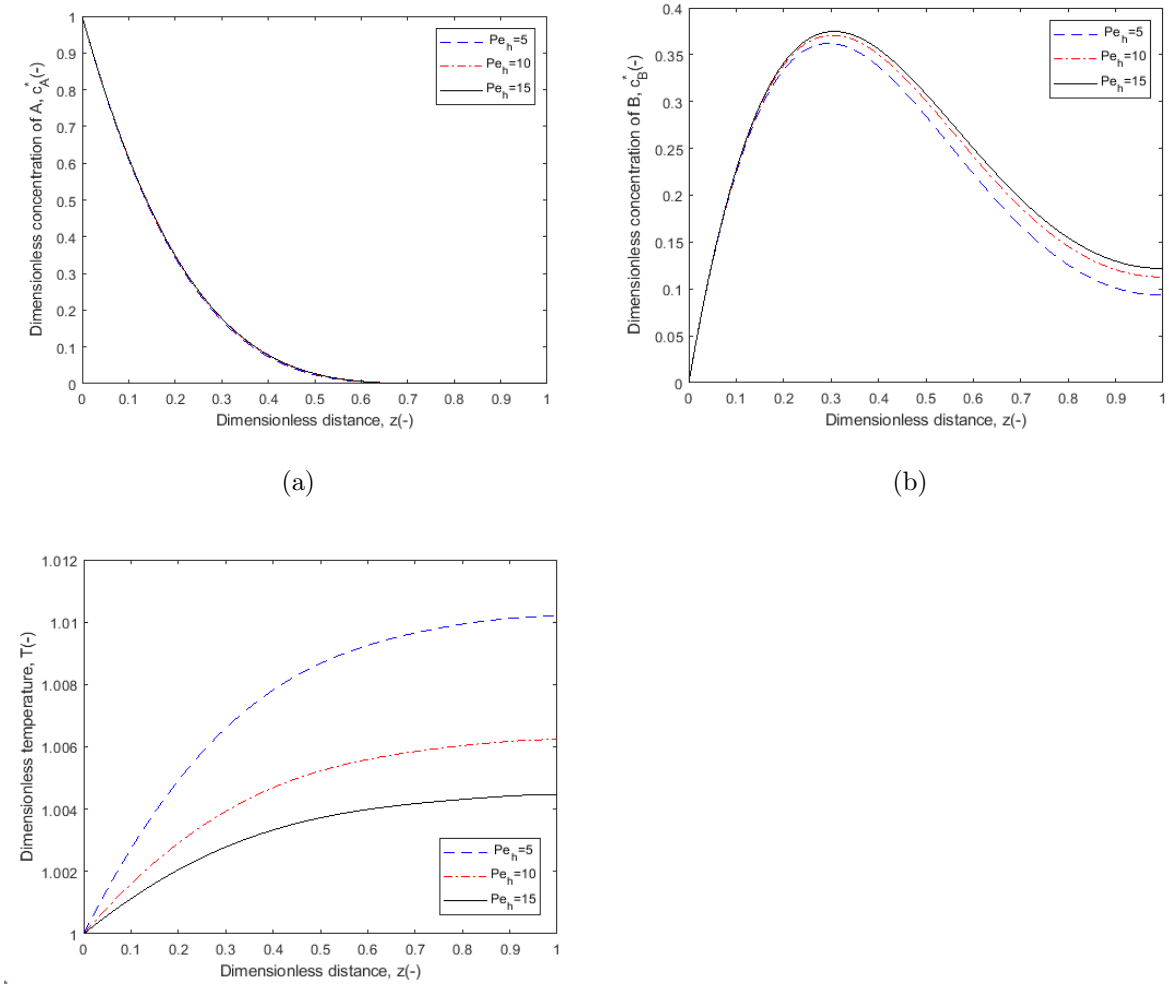

Figure 4-2: Solution profiles without dead-core $|p| > 1, \phi < \phi^*$ simulated for model parameters $Pe_m = 1, p = 0.5, \phi = 2.2$.

In Fig. 4-1(b), it is shown that the lower Peclet number, $Pe_m = 5$, corresponds to the higher dimensionless concentration of product B profile until some point in distance, then the highest Peclet number, 15, corresponds to the higher concentration profile until the end. It is changed because of the formation of dead zone for the component A. In Fig. 4-1(c), the lowest Peclet number corresponds to the highest dimensionless temperature value.

In comparison with Fig. 4-1, Fig. 4-2 shows the effect of the heat Peclet number Pe_h on the solutions. It is worth noting that in Fig. 4-2(a) dimensionless concentration of A was not affected by change of Pe_h. In Fig. 4-2(b) and 4-2(c), the situations are opposite to each other. While the concentration profile of B increases with increasing values of Pe_h, the temperature decreases.

4.1.2 Effects of Thiele Modulus

The effect of Thiele modulus plays one of the important role in determination of the dead zones. It is important to know a priori where the zone appears. Dead core is a zone where no reaction and fully consumption of reactants occur [15]. This may result in an inefficient use of expensive catalysts [16], [10].

As mentioned above Andreev [5] formulated necessary conditions for existing of the dead zones. In our case they are $|p| < 1$ and since the reaction orders eare assumed to be equal $p_A = p_B$, the dead core for the component B appears after formation of such a zone by reactant A. This could be seen from Fig. 4-3(a) and Fig. 4-3(b). After formation of dead zones in Fig. 4-3(a) with $\phi = 2$ and $\phi = 1.5$, the graphs in Fig. 4-3(b) for the same Thiele modulus changed their trend which is also shown in Fig. 4-1 and Fig. 4-2. Andreev, Skrzypacz, and Golman [12] discussed the sufficient condition $\phi \geq \phi^*$ for temperature-dependent reaction, by derivation and numerical analysis of the critical Thiele modulus ϕ^*. It depends on several parameters, such as reaction order, Arrhenius numbers γ_1, γ_2, Prater numbers β_1, β_2. In the exothermic case ($\beta > 0$), the bigger Arrhenius number leads to the higher temperature, while in the endothermic case ($\beta < 0$) it has opposite situation. Thus it causes for exothermic reaction the lower critical Thiele modulus and for endothermic the higher [12].

The concentration of the components A (a),B (b) and temperature (c) profiles variations with Thiele modulus are illustrated in Fig. 4-3. By decreasing of Thiele modulus, the concentration of A increases, as shown in Fig. 4-3(a). The reaction order is equal to 0.5, which satisfies necessary condition, and for values $\phi \geq \phi^*$: 1.5, 2 dead-core appears in Fig. 4-3(a). In Fig. 4-3(b), since the dead zone is appeared in (a), the trend is changed for $\phi = 1.5$ and $\phi = 2$, as said above. In order to have dead zone for concentration of B, there other higher values of Thiele modulus are needed. In the graph in Fig. 4-3(c) the temperature profile decreases with increasing Thiele modulus.

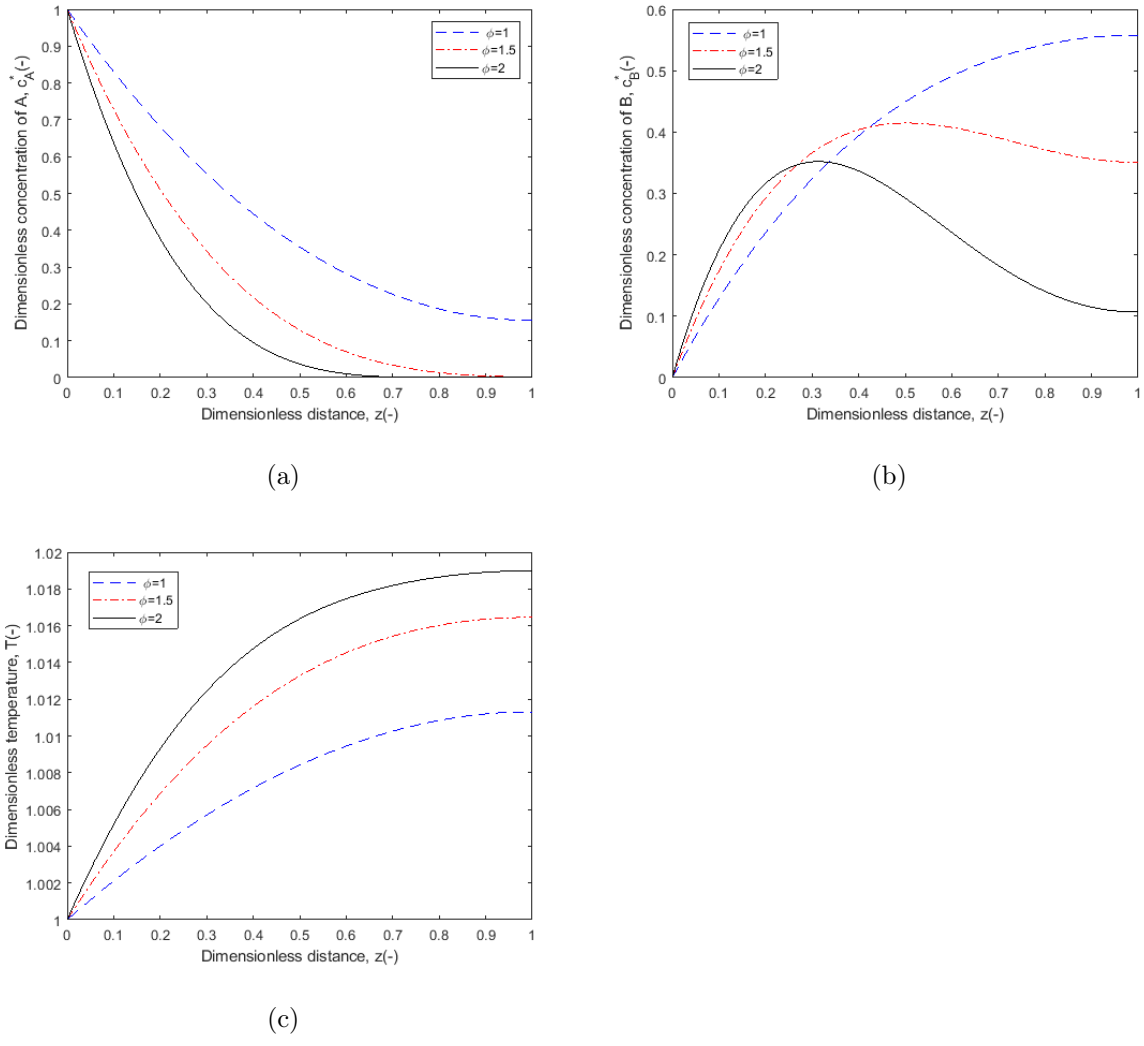

Figure 4-3: The concentration of (a)A and (b)B, and (c)temperature profiles for dead-core problem with parameters $Pe_m = 1, Pe_h = 1, p = 0.5$.

4.1.3 Effects of the Reaction Order

As already stated, reaction order has an effect on critical Thiele modulus. As reaction order p increases, so does critical Thiele modulus and vice versa [5], [10], [17].

The Fig. 4-4 and Fig. 4-5 describe solution profiles in the cases, when there is no dead-core for reaction orders $|p| > 1$ & $|p| < 1$, respectively. In Fig. 4-5(a) and 4-5(b), the case is illustrated when the necessary condition for dead-core existence, $|p| < 1$, is satisfied, whereas the sufficient condition $\phi < \phi^*$ is violated.

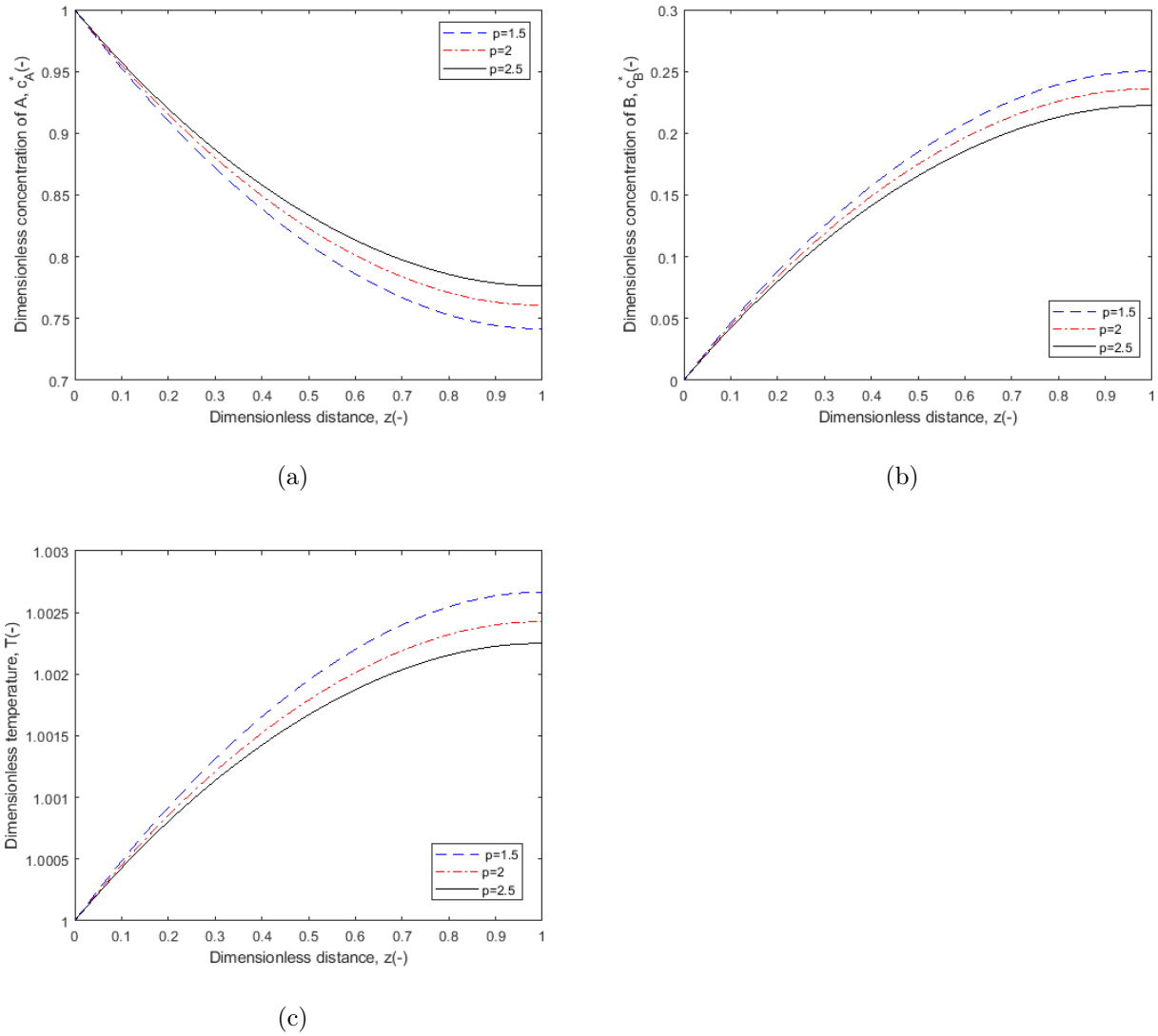

Figure 4-4: The concentration of A and B, and temperature profiles without dead-core $|p| > 1, Pe_m = 1, Pe_h = 1, \phi = 0.5$.

Fig. 4-4(a) and Fig. 4-5(a) illustrate the similar trend. The concentration of reactant A, in both situations, decreases faster with decreasing reaction orders. In Fig. 4-4(b) with concentration of product B, the lower values of reaction orders match with higher concentrations. Also, concentration of A goes down, while concentration of B goes up at the dimensionless distance, $z = 1$. The temperature profiles in both Fig. 4-4 and 4-5 increases over x axis and has higher values for the lower reaction rates.

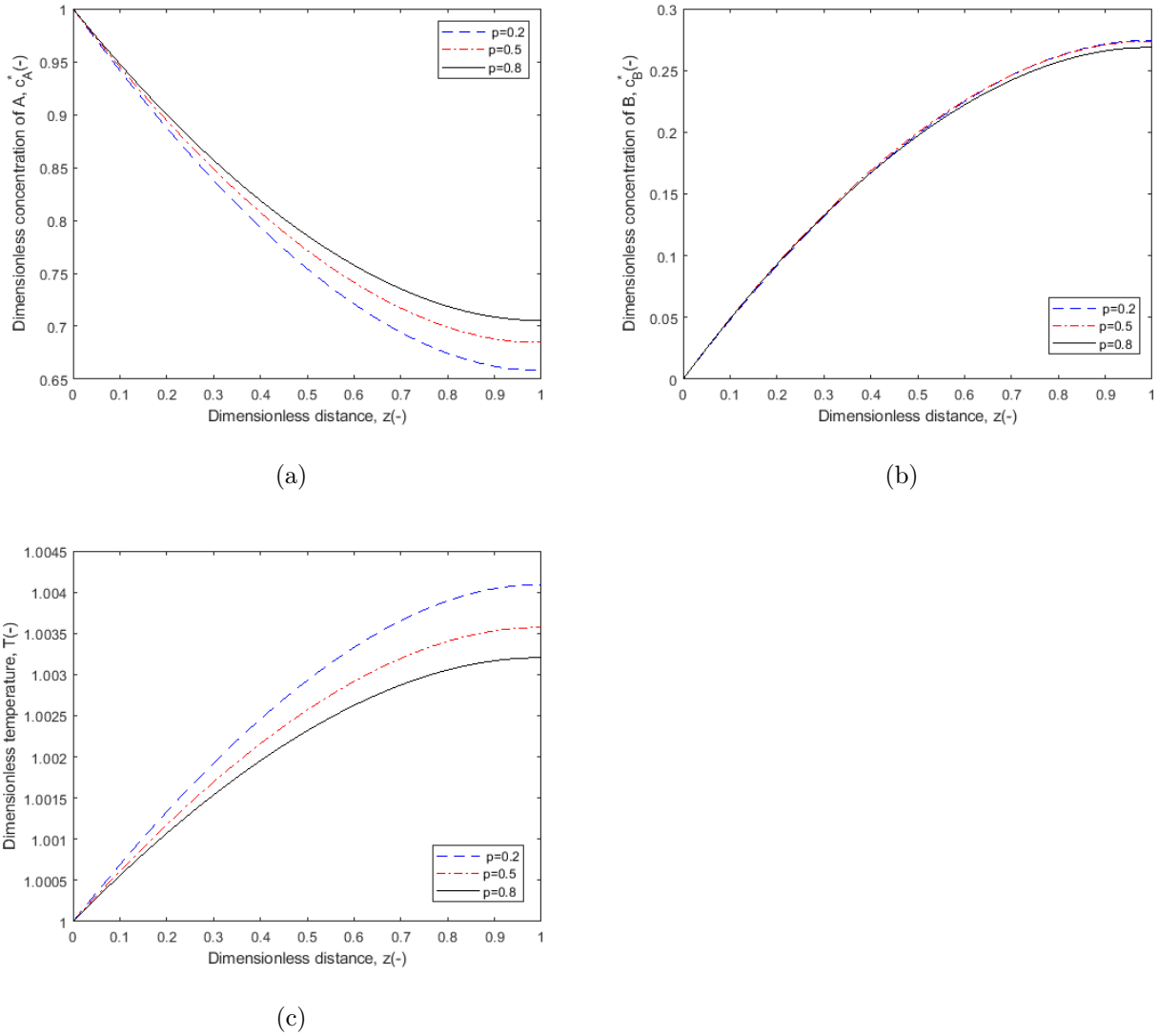

Figure 4-5: The concentration of A and B, and temperature profiles without dead-core, $\phi < \phi*, |p| < 1, Pe_m = 1, Pe_h = 1, \phi = 0.5$.

Dead zone is appeared for both concentrations of A and B, as represented in

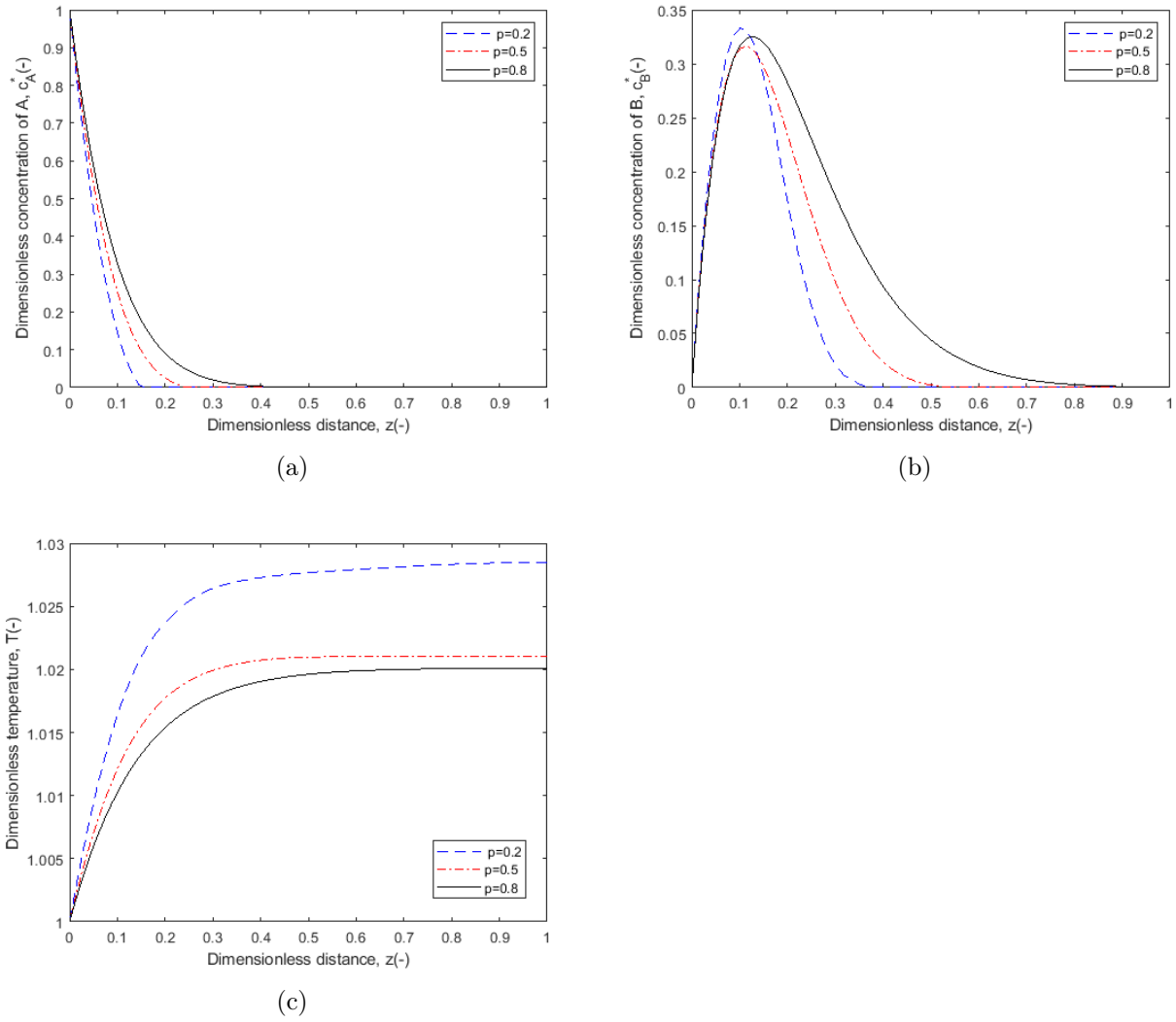

Figure 4-6: The concentration of A and B, and temperature profiles for dead-core problem $Pe_m = 1, Pe_h = 1, \phi = 5$.

Fig. 4-6. Thiele modulus was set to $\phi = 5$. As reaction order decreases, length of the dead zones increases. Also, the dead zone temperature appears in the Fig. 4-6(c). As seen from the graph, the temperature is a constant after some distance.

4.2 Conversion, Selectivity and Yield

In order to study the reactor performance, we considered conversion, selectivity and yield profiles.

To remind, conversion of reactant A, selectivity of intermediate product B, and

yield of B component are given as follows, respectively:

$$X = 1 - c^*_{A,L} \tag{4.1}$$

$$S = \frac{c^*_{B,L}}{1 - c^*_{A,L}} \tag{4.2}$$

$$Y = S * X \tag{4.3}$$

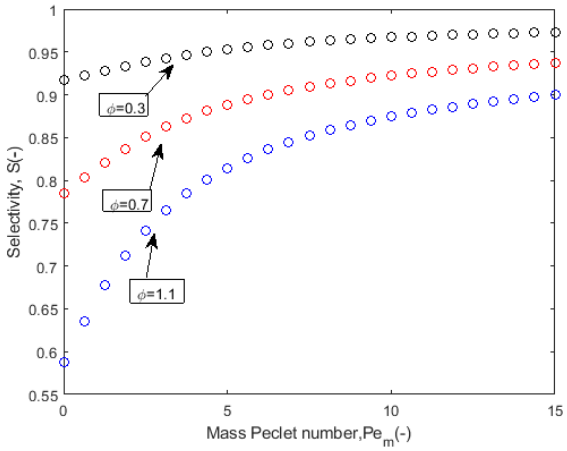

(a)

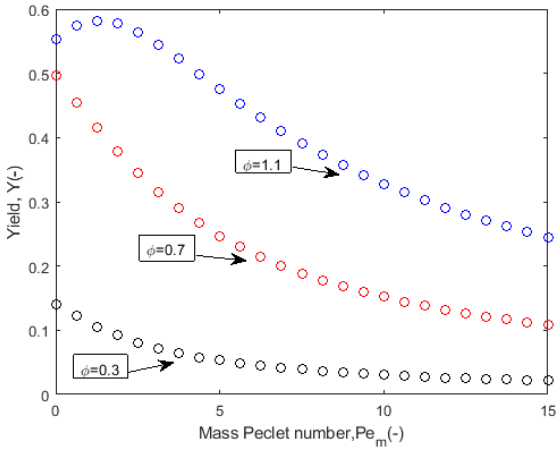

(b)

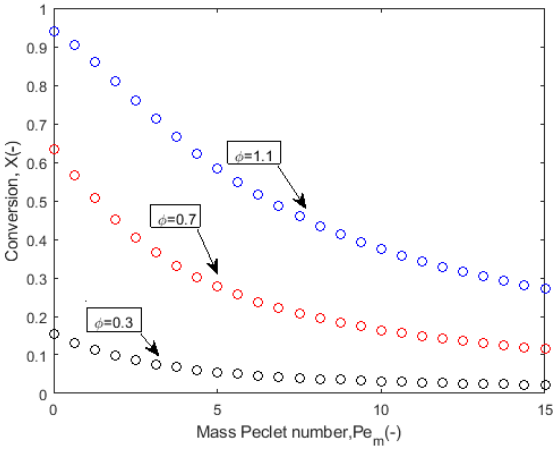

(c)

Figure 4-7: Dependency of selectivity, yield and conversion on Pe_m in isothermal case for $Pe_h = 1, p = 0.5$

Fig. 4-7 illustrates the dependence of selectivity, yield of B and conversion on different values of mass Peclet number and Thiele modulus in isothermal reaction. In Fig. 4-7(a), by increasing of Pe_m selectivity of intermediate product B increases whereas an increase in Thiele modulus corresponds to the decrease of selectivity. It

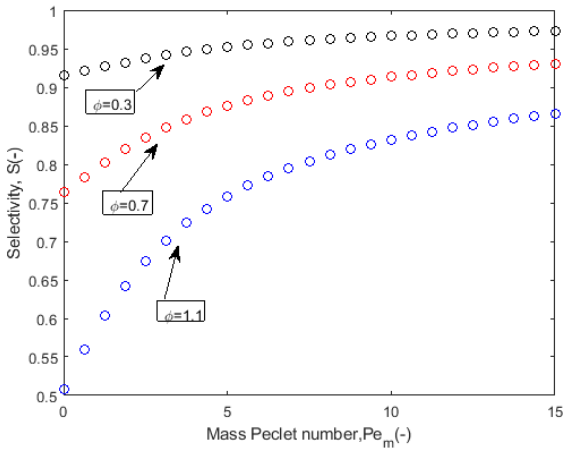

(a)

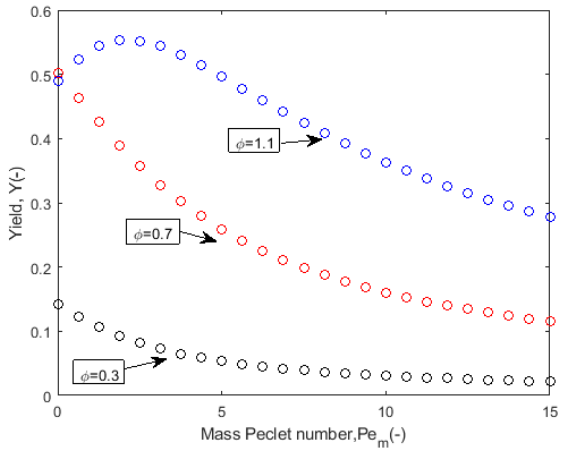

(b)

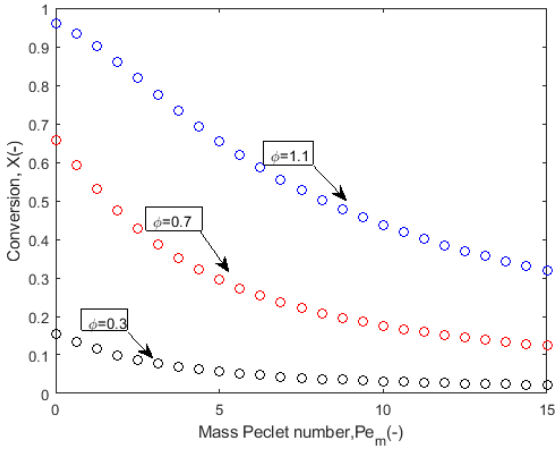

(c)

Figure 4-8: Dependency of selectivity and yield on Pe_m in nonisothermal case for $Pe_h = 0, p = 0.1$.

has opposite trend in Fig. 4-7(c) for the lower Thiele modulus, conversion is also lower and an increase of Peclet number results in a decline of conversion. It means that selectivity and conversion are inversely proportional to each other. In Fig. 4-7(b) shows effect of Peclet number on yield. From the graph it is recognizable that for the lower values of Thiele modulus $\phi = 0.3, \phi = 0.7$ yield decreases with increasing Pe_m.

But for $\phi = 1.1$, there is an increase in yield with increasing Pe_m for certain values of Pe_h and then it decreases. At the $Pe_m = 15$, line with the highest Thiele modulus has the biggest yield, approximately $Y = 0.25$. These graphs illustrates isothermal reaction, where temperature is constant.

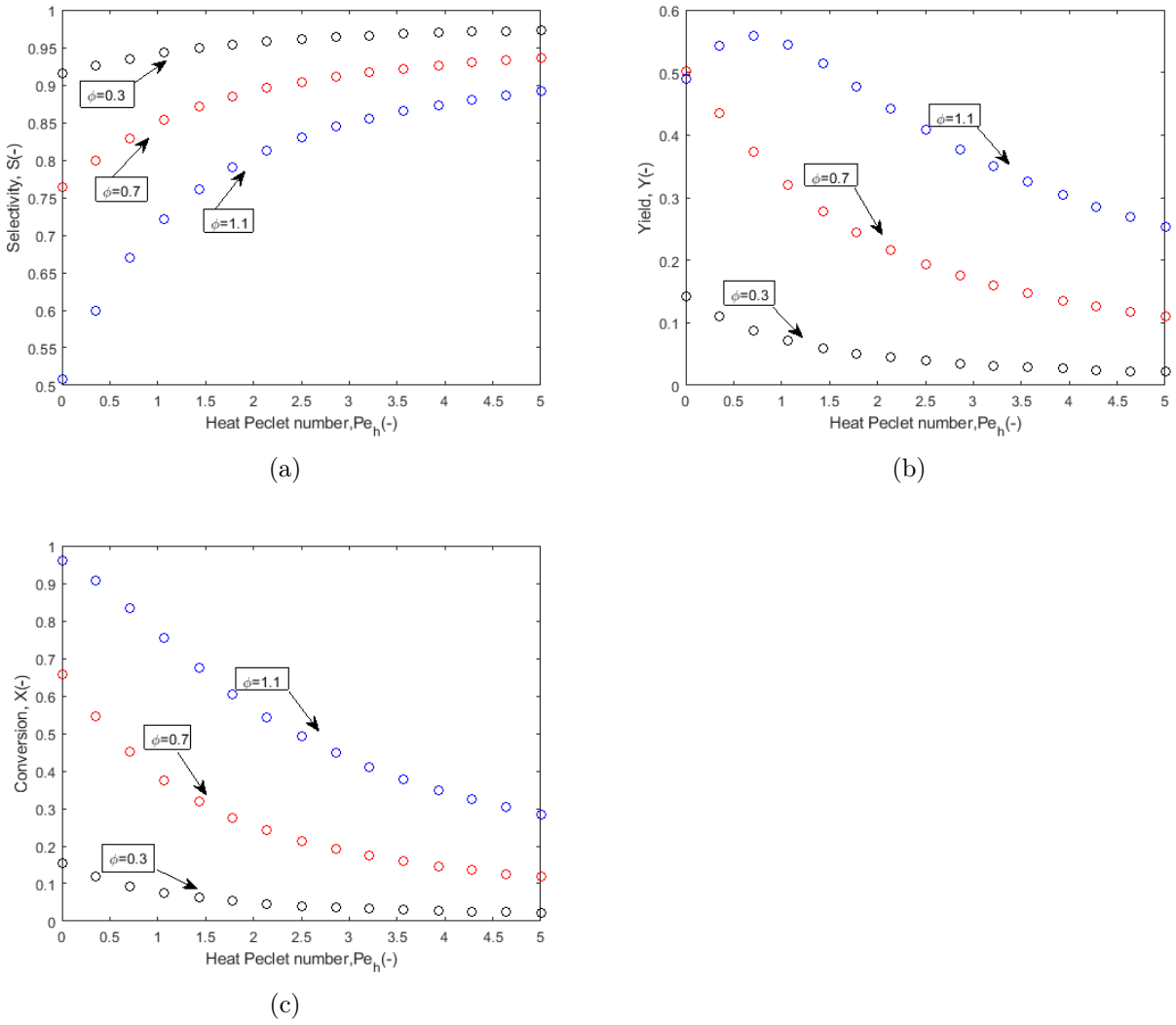

Figure 4-9: Dependency of selectivity, yield and conversion on Pe_h in nonisothermal case with $Pe_m/Pe_h = 3, p = 0.5$

Nonisothermal condition are considered in Fig. 4-8 and Fig. 4-9. Fig. 4-8 depends on Pe_m, while Fig. 4-9 on Pe_h. In comparison with Fig. 4-7 under the isothermal condition, the results for selectivity, yield and conversion almost the same. However, selectivity with Thiele modulus $\phi = 1.1$ at point $Pe_m = 0$ is between 0.55 and 06,

as shown in Fig. 4-7(a). In Fig. 4-8 and 4-9, selectivity for this ϕ starts from 0.5. Accordingly, yields with $\phi = 1.1$ has differences at the lower values of Peclet numbers. Despite the fact that in Fig. 4-7 $Pe_h = 0$ and in Fig. 4-8 $Pe_h = Pe_m * 3$, in both figures curves show the same trends.

In comparison with the figures for the selectivity and yield of the intermediate product in the paper of Golman, Shinohara and Kobayashi [6], performance in this study is worse. In their work, linear kinetics ($p = 1$)is used for both components A and B, while in this thesis power-law kinetics was considered. The graphs for selectivity show similarities in both works, where the lower Thiele modulus ϕ leads to the higher selectivity and the conversion shows the opposite trend.

Chapter 5

Conclusion and Outlooks

The mathematical model for the Cathalytic Membrane Reactor (CMR) was based on the one-dimensional convection-diffusion-reaction equations presented by Golman at al. [6]. In the present work, the reaction term was of power-law type with fractional exponent, and the model described an irreversible exothermic reaction in the porous membrane reactor with catalysts impregnated inside the walls of the pores. The desired product was an intermediate in the consecutive reaction.

This work was aimed to solve numerically the convection-diffusion-reaction problem for CMR. To study the system of nonlinear steady-state partial differential equations with boundary conditions, numerical approach based on Finite Difference Method and the modified Crank-Nicolson scheme was applied. The correctness of the numerical results was verified by the collocation-based pdepe Matlab solver [7]. Pdepe Matlab solver fails for large values of some system parameters while the proposed Crank-Nicolson method copes with that parameter limitation. It produces stable numerical solutions for the large Thiele modulus parameters. Moreover, the proposed method has unconditional stability and second-order of accuracy in both space and time.

The presense of reaction terms corresponding to the power-law kinetics with fractional order between 0 and 1 can lead to the formation of dead zones. Parameter study showed that the concentration increases and temperature decreases with increasing mass Peclet number, while in the case with different heat Peclet numbers the trend

for the concentration remains the same. It is concluded that for every component A and B, there are some critical values of Thiele modulus for the formation of dead core. This finding is supported by the necessary conditions discussed by Andreev [5] for a consecutive irreversible reaction. By the increase of Thiele modulus, concentration decreases, and temperature increases. The effects of reaction order have an opposite tendency for both of them. The length of the dead zones increases with decreasing Peclet number and reaction order, and with increasing Thiele modulus. The performance of the model reactor with respect to the conversion, selectivity, and yield of the product was studied. The obtained results are important for desing of efficient chemical reactors since the knowledge about the appearance of dead cores can significantly reduce reactor fabrication costs caused by expensive catalysts.

Many analytical and numerical results on the formation of dead zones have been established for models based on diffusion-reaction equations. The critical Thiele modulus was derived mainly for the simple catalytic reaction equations. In this study, the effect of convection is also considered. More investigations of dead core solutions to convection-diffusion-reaction problems could lead to new applicable results. Furthermore, rigorous error analysis of the Crank-Nicolson method should be performed for these problems, and instead of the Finite Difference Method, the Finite Element Method (FEM) for the spatial discretization can be used in the forthcoming works.

Chapter 6

Appendix

6.1 Appendix A: Matlab Code

6.1.1 Code for the Concentration of A,B and Temerature Profiles

```
% solving 1d dead-core problem
%  u_t-u''+Pe*u'+ phi^2*xi/psi*exp(gamma1*(1-1/T)*u^p = 0  in
    (0,1)
%  v_t-v''+Pe*v'- phi^2*xi*exp(gamma1*(1-1/T)*u^p +phi^2*exp(
   gamma2*(1-1/T))*v^p= 0
%  T_t-T''+Peh*T'- beta1*phi^2*xi/psi*exp(gamma1*(1-1/T)*u^p
   -beta2*phi^2*exp(gamma2*(1-1/T)*v^p= 0
%   BC's:
%  u(t,0) =T(t,0)= 1, v(t,0)=0,
%  u_x(t,1) =v_x(t,1)=T_x(t,1)= 0  for t in (0,1)
%   IC's:
%  u(0,x) =v(0,x)=T(0,x)= 1
close all;
p=0.5; %reaction exponent
Pe=1; %mass Peclet number
Peh=1; %heat Peclet number
```

```
14 phi=0.5; %Thiele modulus
15
16 %Constant parameters
17 psi=1; %diffusivity ratio
18 xi=4; %reaction rate ratio
19 beta1=0.01; %Prater numbers beta1 and beta2
20 beta2=0.01;
21 gamma1=10; %Arrhenius numbers gamma1 and gamma2 for A and B,
       respectively
22 gamma2=20;
23
24 % number of spatial grid points N>=2
25 Nx=70;
26 % generate spatial grid points
27 x=linspace(0,1,Nx);
28 % spatial mesh size
29 hx=1/(Nx-1);
30
31 % number of temporal grid points N>=2
32 Nt=350;
33 t=linspace(0,1,Nt);
34 % temoral mesh size
35 tau=1/(Nt-1);
36
37 % allocate the stiffnes matrix
38 A = sparse([],[],[],Nx-2,Nx-2,(Nx-2)*3); %for first
       concentration (u) equation
39 B = sparse([],[],[],Nx-2,Nx-2,(Nx-2)*3);  %for third(
       temperature) equation
40 C = sparse([],[],[],Nx-2,Nx-2,(Nx-2)*3); %for second
```

```
    concentration (c) equation

41
42 % identity matrix
43 I = speye(Nx-2, Nx-2);
44
45 % Laplacian
46 %u"
47 A=1/((hx)^2)*sparse(-diag(2*ones(Nx-2,1))+diag(ones(Nx-3,1)
       ,1)+diag(ones(Nx-3,1),-1));
48 % backward differences for u'
49 A=A-Pe/(hx)*sparse(diag(ones(Nx-2,1))+diag((-1)*ones(Nx-3,1)
       ,-1));
50
51 %T"
52 B=1/((hx)^2)*sparse(-diag(2*ones(Nx-2,1))+diag(ones(Nx-3,1)
       ,1)+diag(ones(Nx-3,1),-1));
53 % backward differences for T'
54 B=B-Peh/(hx)*sparse(diag(ones(Nx-2,1))+diag((-1)*ones(Nx-3,1)
       ,-1));
55
56 %c"
57 C=1/((hx)^2)*sparse(-diag(2*ones(Nx-2,1))+diag(ones(Nx-3,1)
       ,1)+diag(ones(Nx-3,1),-1));
58 % backward differences for c'
59 C=C-Pe*psi/(hx)*sparse(diag(ones(Nx-2,1))+diag((-1)*ones(Nx
       -3,1),-1));
60
61 %Dirichlet BC's
62 ua=1;
63 Ta=1;
```

```
64 ca=0;
65
66 % modify zero rhs because of Dirichlet b.c.'s
67 fu=zeros(Nx-2,1);
68 fu(1)=1/(hx^2)+Pe/hx;
69 fT=zeros(Nx-2,1);
70 fT(1)=1/(hx^2)+Peh/hx;
71 fc=zeros(Nx-2,1);
72
73 % applying Neumann b.c.'s
74 A(Nx-2,Nx-2)=A(Nx-2,Nx-2)+1/hx^2;
75 B(Nx-2,Nx-2)=B(Nx-2,Nx-2)+1/hx^2;
76 C(Nx-2,Nx-2)=C(Nx-2,Nx-2)+1/hx^2;
77
78 %IC's
79 Told=ones(Nx-2,1);
80 uold=ones(Nx-2,1);
81 cold=zeros(Nx-2,1);
82
83 % fixed-point iteration at each time step
84 unew=zeros(Nx-2,1);
85 Tnew=zeros(Nx-2,1);
86 cnew=zeros(Nx-2,1);
87
88 % time stepping
89 unew_new=zeros(Nx-2,1);
90 Tnew_new=zeros(Nx-2,1);
91 cnew_new=zeros(Nx-2,1);
92
93 % for plotting
```

```
94  ufull=zeros(Nx,1);
95  Tfull=zeros(Nx,1);
96  cfull=zeros(Nx,1);
97
98  for i=1:Nt
99     %fixed-point iteration step of Crank-Nicolson
100 for j=1:2
101     unew=(I-1/2*tau*A)\(uold+1/2*tau*A*uold-1/2*tau*phi^2*xi/
            psi*exp(gamma1*(1-1./Told)).*(max(unew,0).^p+max(uold
            ,0).^p)+tau*fu);
102     cnew=(I-1/2*tau*C)\(cold+1/2*tau*C*cold+tau*xi*phi^2*exp(
            gamma1*(1-1./Told)).*max(uold,0).^p-1/2*tau*phi^2*exp(
            gamma2*(1-1./Told)).*(max(cnew,0).^p+max(cold,0).^p));
103     Tnew=(I-1/2*tau*B)\(Told+1/2*tau*B*Told+1/2*tau*beta1*xi/
            psi*phi^2*(exp(gamma1*(1-1./Tnew))+exp(gamma1*(1-1./
            Told))).*max(uold,0).^p+1/2*tau*beta2*phi^2*(exp(gamma2
            *(1-1./Tnew))+exp(gamma2*(1-1./Told))).*max(cold,0).^p+
            tau*fT);
104
105     uold=0.5*max(unew,0)+0.5*max(uold,0);
106     cold=0.5*max(cnew,0)+0.5*max(cold,0);
107     Told=0.5*max(Tnew,0)+0.5*max(Told,0);
108 end
109 unew_new=max(unew,0);
110 cnew_new=max(cnew,0);
111 Tnew_new=max(Tnew,0);
112
113 ufull(1)=ua;
114 ufull(2:Nx-1)=unew_new;
115 ufull(Nx)=unew_new(Nx-2);
```

```
116
117 cfull(1)=ca;
118 cfull(2:Nx-1)=cnew_new;
119 cfull(Nx)=cnew_new(Nx-2);
120
121 Tfull(1)=Ta;
122 Tfull(2:Nx-1)=Tnew_new;
123 Tfull(Nx)=Tnew_new(Nx-2);
124 end
125 figure(1)
126 plot(x,ufull);
127 xlabel('Dimensionless distance, z(-)');
128 ylabel('Dimensionless concentration, c_A(-)');
129
130 figure(2)
131 plot(x,Tfull);
132 xlabel('Dimensionless distance, z(-)');
133 ylabel('Dimensionless temperature, \theta(-)');
134
135 figure(3)
136 plot(x,cfull);
137 xlabel('Dimensionless distance, z(-)');
138 ylabel('Dimensionless concentration, c_B(-)');
```

6.1.2 Code for plotting Selectivity, Yield, and Conversion under Non-isothermal Condition

```
% solving 1d dead-core problem
%  u_t-u''+Pe*u'+ phi^2*xi/psi*exp(gamma1*(1-1/T)*u^p = 0  in (0,1)
%  v_t-v''+Pe*v'- phi^2*xi*exp(gamma1*(1-1/T)*u_+^p +phi^2*exp(gamma2*(1-1/T))*v^p= 0
%  T_t-T''+Peh*T'- beta1*phi^2*xi/psi*exp(gamma1*(1-1/T)*u^p-beta2*phi^2*exp(gamma2*(1-1/T)*v^p= 0
%   BC's:
%  u(t,0) =T(t,0)= 1, v(t,0)=0,
%  u_x(t,1) =v_x(t,1)=T_x(t,1)= 0  for t in (0,1)
%   IC's:
%  u(0,x) =v(0,x)=T(0,x)= 1
close all;
p=0.5; %reaction exponent
Peh=1; %heat Peclet number
phi=0.3; %Thiele modulus

%Constant parameters
psi=1;
xi=4;
beta1=0.01; %Prater numbers beta1 and beta2
beta2=0.01;
gamma1=10;
gamma2=20;

% number of spatial grid points N>=2
Nx=70;
```

```
25
26 % generate spatial grid points
27 x=linspace(0,1,Nx);
28
29 % spatial mesh size
30 hx=1/(Nx-1);
31
32 % number of temporal grid points N>=2
33 Nt=350;
34 t=linspace(0,1,Nt);
35
36 % temoral mesh size
37 tau=1/(Nt-1);
38
39 % allocate the stiffnes matrix
40 A = sparse([],[],[],Nx-2,Nx-2,(Nx-2)*3); %for first
     concentration (u) equation
41 B = sparse([],[],[],Nx-2,Nx-2,(Nx-2)*3);  %for third(
     temperature) equation
42 C = sparse([],[],[],Nx-2,Nx-2,(Nx-2)*3); %for second
     concentration (c) equation
43
44 % identity matrix
45 I = speye(Nx-2, Nx-2);
46
47 while phi<=1.1
48  for Pe=linspace(0,15,25) %Different values for mass Peclet
      number
49 % Laplacian
50 %u"
```

```
51 A=1/((hx)^2)*sparse(-diag(2*ones(Nx-2,1))+diag(ones(Nx-3,1)
       ,1)+diag(ones(Nx-3,1),-1));
52 % backward differences for u'
53 A=A-Pe/(hx)*sparse(diag(ones(Nx-2,1))+diag((-1)*ones(Nx-3,1)
       ,-1));
54
55 %T"
56 B=1/((hx)^2)*sparse(-diag(2*ones(Nx-2,1))+diag(ones(Nx-3,1)
       ,1)+diag(ones(Nx-3,1),-1));
57 % backward differences for T'
58 B=B-Peh/(hx)*sparse(diag(ones(Nx-2,1))+diag((-1)*ones(Nx-3,1)
       ,-1));
59
60 %c"
61 C=1/((hx)^2)*sparse(-diag(2*ones(Nx-2,1))+diag(ones(Nx-3,1)
       ,1)+diag(ones(Nx-3,1),-1));
62 % backward differences for c'
63 C=C-Pe*psi/(hx)*sparse(diag(ones(Nx-2,1))+diag((-1)*ones(Nx
       -3,1),-1));
64
65 %Dirichlet BC's
66 ua=1;
67 Ta=1;
68 ca=0;
69
70 % modify zero rhs because of Dirichlet b.c.'s
71 fu=zeros(Nx-2,1);
72 fu(1)=1/(hx^2)+Pe/hx;
73 fT=zeros(Nx-2,1);
74 fT(1)=1/(hx^2)+Peh/hx;
```

```
75 fc=zeros(Nx-2,1);
76
77 % applying Neumann b.c.'s
78 A(Nx-2,Nx-2)=A(Nx-2,Nx-2)+1/hx^2;
79 B(Nx-2,Nx-2)=B(Nx-2,Nx-2)+1/hx^2;
80 C(Nx-2,Nx-2)=C(Nx-2,Nx-2)+1/hx^2;
81
82 %IC's
83 Told=ones(Nx-2,1);
84 uold=ones(Nx-2,1);
85 cold=zeros(Nx-2,1);
86
87 % fixed-point iteration at each time step
88 unew=zeros(Nx-2,1);
89 Tnew=zeros(Nx-2,1);
90 cnew=zeros(Nx-2,1);
91
92 % time stepping
93 unew_new=zeros(Nx-2,1);
94 Tnew_new=zeros(Nx-2,1);
95 cnew_new=zeros(Nx-2,1);
96
97 % for plotting
98 ufull=zeros(Nx,1);
99 Tfull=zeros(Nx,1);
100 cfull=zeros(Nx,1);
101
102 for i=1:Nt
103    %fixed-point iteration step of Crank-Nicolson
104 for j=1:2
```

```
105     unew=(I-1/2*tau*A)\(uold+1/2*tau*A*uold-1/2*tau*phi^2*xi/
            psi*exp(gamma1*(1-1./Told)).*(max(unew,0).^p+max(uold
            ,0).^p)+tau*fu);
106     cnew=(I-1/2*tau*C)\(cold+1/2*tau*C*cold+tau*xi*phi^2*exp(
            gamma1*(1-1./Told)).*max(uold,0).^p-1/2*tau*phi^2*exp(
            gamma2*(1-1./Told)).*(max(cnew,0).^p+max(cold,0).^p));
107     Tnew=(I-1/2*tau*B)\(Told+1/2*tau*B*Told+1/2*tau*beta1*xi/
            psi*phi^2*(exp(gamma1*(1-1./Tnew))+exp(gamma1*(1-1./
            Told))).*max(uold,0).^p+1/2*tau*beta2*phi^2*(exp(gamma2
            *(1-1./Tnew))+exp(gamma2*(1-1./Told))).*max(cold,0).^p+
            tau*fT);
108
109     uold=0.5*max(unew,0)+0.5*max(uold,0);
110     cold=0.5*max(cnew,0)+0.5*max(cold,0);
111     Told=0.5*max(Tnew,0)+0.5*max(Told,0);
112 end
113
114 unew_new=max(unew,0);
115 cnew_new=max(cnew,0);
116 Tnew_new=max(Tnew,0);
117
118 ufull(1)=ua;
119 ufull(2:Nx-1)=unew_new;
120 ufull(Nx)=unew_new(Nx-2);
121
122 cfull(1)=ca;
123 cfull(2:Nx-1)=cnew_new;
124 cfull(Nx)=cnew_new(Nx-2);
125
126 Tfull(1)=Ta;
```

```
127 Tfull(2:Nx-1)=Tnew_new;
128 Tfull(Nx)=Tnew_new(Nx-2);
129 end
130 X=(1-ufull(Nx)); %Conversion
131 Sel=cfull(Nx)/(X); %Selectivity
132 Y=X*Sel; %Yield
133
134 figure(1);
135 for M = 1 : 3
136 if phi==0.3
137     plot(Pe,Sel,'oblack');
138 elseif phi==0.7
139     plot(Pe,Sel,'or');
140 else
141     plot(Pe,Sel,'ob');
142 end
143  xlabel('Mass Peclet number,Pe_m(-)');
144  ylabel('Selectivity, S(-)');
145  hold on
146 end
147
148 figure(2);
149 for K = 1 : 3
150 if phi==0.3
151     plot(Pe,Y,'oblack');
152 elseif phi==0.7
153     plot(Pe,Y,'or');
154 else
155     plot(Pe,Y,'ob');
156 end
```

```
157  xlabel('Mass Peclet number,Pe_m(-)');
158  ylabel('Yield, Y(-)');
159  hold on
160 end
161
162 figure(3);
163 for L = 1 : 3
164 if phi==0.3
165     plot(Pe,X,'oblack');
166 elseif phi==0.7
167     plot(Pe,X,'or');
168 else
169     plot(Pe,X,'ob');
170 end
171  xlabel('Mass Peclet number,Pe_m(-)');
172  ylabel('Conversion, X(-)');
173  hold on
174 end
175 end
176  phi=phi+0.4;
177 end
```

Bibliography

[1] Matson S.L., Quinn J.A. (1992) *Membrane Reactors.* In: Ho W.S.W., Sirkar K.K. (eds) Membrane Handbook. Springer, Boston, MA

[2] Seidel-Morgenstern, A. (Ed.). (2010). *Membrane reactors: distributing reactants to improve selectivity and yield.* In IEEE International John Wiley & Sons.

[3] Basile, A., and Gallucci, F. (Eds.). (2010). *Membranes for membrane reactors: preparation, optimization and selection.* John Wiley & Sons.

[4] Tan, X. *Inorganic Membrane Reactors, Second edition.;* Wiley: China, UK, 2015; pp 1- 25, 143-179.

[5] Andreev, V. V. (2013) . *Formation of a "dead zone" in porous structures during processes that proceeding under steady-state and unsteady-state conditions.* Review Journal of Chemistry, 3(3), 239-269.

[6] Golman, B., Shinohara, K., & Kobayashi, M. (1997). *Selectivity and yield of exothermic consecutive reactions in catalytically active porous membrane reactor.* Journal of chemical engineering of Japan, 30(3), 507-513.

[7] MATLAB. Natick, MA: The Math Works, Inc.;2018.

[8] Seel RD, Berzins M. *A method for the spatial discretization of parabolic equations in one space variable.* SIAM J Sci Comput. 1990;11:1-32.

[9] Beers, K. J.(2007). *Numerical methods for chemical engineering: applications in Matlab.* Cambridge University Press.

[10] Sabit, F., Shakipov, M., Skrzypacz, P., & Golman, B. (2019). *Dead-core solutions to simple catalytic reaction problems in chemical engineering.* Eurasian Chemico-Technological Journal, 21(1), 29-33.

[11] Skrzypacz, P., Andreev, V. V., and Golman, B. (2020). *Dead-core and non-dead-core solutions to diffusion-reaction problems for catalyst pellets with external mass transfer.* Chemical Engineering Journal, 385, 123927.

[12] Andreev, V. V., Skrzypacz, P., and Golman, B. (2019). *The formation of dead zones in nonisothermal porous catalyst with temperature-dependent diffusion coefficient.* International Journal of Chemical Kinetics, 51(9), 711-722.

[13] Kruczek B. (2015) *Convective Transport.* In: Drioli E., Giorno L. (eds) Encyclopedia of Membranes. Springer, Berlin, Heidelberg

[14] Gu, Y., Bacchin, P., Lahitte, J. F., Remigy, J. C., Favier, I., Gomez, M., and Noble, R. D. (2017). *Catalytic membrane reactor for Suzuki-Miyaura C- C cross-coupling: Explanation for its high efficiency via modeling.* AIChE Journal,63(2),698-704.

[15] Temkin, M. I. (1975). *Diffusion effects during the reaction on the surface pores of a spherical catalyst particle.* Kinet. Catal, 16, 104-112.

[16] Aris, R. (1975). *The Mathematical Theory of Diffusion and Reaction in Permeable Catalysts*, vols. I and II. Clarendon.

[17] Koltsov, N. I., & Andreev, V. V. (1995). *Peculiarities of simple and complex chemical reactions in grains of porous catalysts.* Kinetics and catalysis, 36(1).

[18] Thongmoon, M., & McKibbin, R. (2006). *A comparison of some numerical methods for the advection-diffusion equation.*